Quaternary Research

doi:10.1017/qua.2020.116

SPECIAL ISSUE
PESAS

Aleutian Low variability for the last 7500 years and its relation to the Westerly Jet

Kana Nagashima[a]*, Jason Addison[b], Tomohisa Irino[c], Takayuki Omori[d], Kei Yoshimura[e], Naomi Harada[a]

[a]Research Institute for Global Change, Japan Agency for Marine-Earth Science and Technology, 2-15 Natsushima-cho, Yokosuka 237-0061, Japan
[b]U.S. Geological Survey, 345 Middlefield Road, Mail Stop 910, Menlo Park, California 94025, USA
[c]Faculty of Environmental Earth Science, Hokkaido University, N10W5 Sapporo, Hokkaido 060-0810, Japan
[d]The University Museum, The University of Tokyo, 7-3-1 Hongo, Bunkyo-ku, Tokyo 113-0033, Japan
[e]Institute of Industrial Science, The University of Tokyo, 5-1-5 Kashiwanoha, Kashiwa, Chiba 277-8574, Japan
*Corresponding author at e-mail: nagashimak@jamstec.go.jp (K. Nagashima)

(Received August 1, 2020; Accepted November 12, 2020)

Abstract

The Aleutian Low (AL) is one of the major atmospheric systems that determines environmental conditions during winter in the North Pacific Ocean, with impacts that affect the climates of both Asia and North America from mid- to high latitudes. However, the multi-centennial and longer scale behavior of the AL during the Holocene is not fully understood. In this study, AL variability since 7.5 ka was examined by applying the principal component analysis technique to published $\delta^{18}O$ data derived from sedimentary calcite, peat, ice, and speleothem from western North America. The extracted Principal Component 1 (PC1) represents a dramatic change from the mid- to late Holocene, and appears to reflect long-term intensified AL related to interactions between orbitally-driven southward shift of the Westerly Jet (WJ) over East Asia and the northwestern Pacific, and intensification of the El Niño–Southern Oscillation. In contrast, PC2 is characterized by multi-centennial to millennial-scale oscillations, with a spatial loading pattern that suggests PC2 reflects AL intensity and position shifts. These oscillations are contemporaneous with both WJ latitude and/or the meandering path shifts over East Asia and solar activity change, suggesting that a decrease/increase in solar irradiance is related to AL variability via interactions with the WJ.

Keywords: Aleutian Low; Westerly Jet; Millennial climate oscillations; Holocene; Pacific Ocean

INTRODUCTION

The history of Holocene climate dynamics is critical for a better understanding of natural climate variability under comparable boundary conditions (e.g., similar ice-sheet sizes, sea level, and atmospheric CO_2 concentrations), particularly prior to the Industrial Revolution. This knowledge is also useful for detecting anthropogenic impacts on climate. However, Holocene climate changes have high spatiotemporal variability (e.g., Mayewski, 2004; Neukom et al., 2019), which complicates achieving a systematic understanding. Therefore, it is essential to extract the characteristic Holocene variation pattern of each component of the climate system to better identify linkages between these components, and to examine the ultimate forcing(s) behind widespread changes in the climate system.

The North Pacific Ocean is the largest geographic feature in the Northern Hemisphere, and its interactions with the overlying atmosphere drives critical components of the global climate system (e.g., Di Lorenzo et al., 2008). The Aleutian Low (AL), the semi-permanent atmospheric low-pressure system centered near the Aleutian Islands, is closely linked to environmental change in the North Pacific and surrounding continental areas. The AL is most intense during the late fall to winter season, and weakens greatly during summer (Beamish and Bouillon, 1993). The average intensity and position of the AL shows large variation at annual and decadal timescales (Overland et al., 1999). This environmental variability occurs at multiple spatial scales, ranging from local effects within the Bering Sea and Gulf of Alaska, to teleconnections with Mexico and the southeastern United States (Latif and Barnett, 1994; Trenberth and Hurrell, 1994; Rodionov et al., 2007). For example, twentieth century decadal variability of the AL intensity and position has been reported to affect salmon abundance in the Northeast Pacific Ocean (Francis and Hare, 1994), Alaskan fjord biogenic sediment accumulation (Addison et al., 2013), and spatial patterns of precipitation across

Cite this article: Nagashima, K., Addison, J., Irino, T., Omori, T., Yoshimura, K., Harada, N. 2022. Aleutian Low variability for the last 7500 years and its relation to the Westerly Jet. *Quaternary Research* 108, 161–179. https://doi.org/10.1017/qua.2020.116

western North America (e.g., Mantua et al., 1997). These complex and wide-ranging effects highlight the need for better understanding of Holocene AL variability and potential impacts under future climate projections.

Paleoclimate reconstructions of Aleutian Low variability

Tree-ring reconstructions describe Pacific environmental variability and associated AL dynamics at the highest levels of spatiotemporal resolution, allowing reconstructions at sub-annual timescales over the recent climate record (e.g., Cook et al., 1999; Biondi et al., 2001; D'Arrigo et al., 2001; MacDonald and Case, 2005; and others). However, these datasets are limited to relatively short time spans, because most of these studies are less than 1000 years old. For timescales that exceed the last 1000 years, AL variations have been interpreted from other, lower time-resolution paleoclimatic proxy archives, such as sodium concentrations in the ice-core dataset from the Mt. Logan summit in Canada (Fisher et al., 2008; Osterberg et al., 2014, 2017). According to Osterberg et al. (2014), the strong surface winds and enhanced uplift during stronger AL phases increases the sea salt concentration in the air that is transported efficiently to Mt. Logan. The correlation between the sodium concentration at Mt. Logan and the North Pacific Index (NPI), which describes the strength of the AL (Trenberth and Hurrell, 1994), over recent instrumental timescales is statistically significant ($r = -0.45$, Osterberg et al., 2014). However, the relatively low correlation value suggests the presence of further factors in addition to AL intensity that may also affect the paleoclimatic interpretation.

Select $\delta^{18}O$ archives preserved in sedimentary calcite, diatom, peat, and speleothems derived from the Aleutian Islands, mainland Alaska, northwestern Canada, and the United States (e.g., Anderson et al., 2005, 2016; Anderson, 2011; Bailey et al., 2018) provide other sources of paleoclimatic insight into Holocene AL behavior based on the interpretation that these records primarily reflect the $\delta^{18}O$ of precipitation due to large-scale atmospheric circulation patterns affected by AL dynamics. Berkelhammer et al. (2012) suggested that intensity and position of the AL control precipitation $\delta^{18}O$ values in North America based on numerical simulations of precipitation $\delta^{18}O$ using the Isotopes-incorporated Global Spectral Model (IsoGSM). The AL variability is closely linked with the Pacific North American (PNA) teleconnection pattern, which is one of the most prominent modes of atmospheric variability over the North Pacific Ocean and North American continent, with the positive phase of the PNA pattern associated with above-average barometric pressure heights in the vicinity of Hawaii and over the intermontane region of North America, and below-average barometric pressure heights located south of the Aleutian Islands (strengthened AL) and over the southeastern United States (Wallace and Gutzler, 1981); the PNA index shows high correlation with simulated $\delta^{18}O$ value in annual and winter precipitation over North America during AD 1950–2005 (Liu et al., 2014), supporting the possible role of AL on the precipitation $\delta^{18}O$ over North America.

Based on the relation between precipitation $\delta^{18}O$ and PNA, Liu et al. (2014) demonstrated possible changes from a negative to positive PNA-like mean state occurred during the mid- to late Holocene using paired $\delta^{18}O$ records from northwestern and southeastern North America, which correspond with a multimillennial-scale shift from a weak to strong AL system. Similar shifts of $\delta^{18}O$ values at around 4 ka have also been documented by Kaufman et al. (2016) from compiled $\delta^{18}O$ records in the northern Gulf of Alaska area (Jellybean Lake, Anderson et al., 2005; Horse Trail Fen, Jones et al., 2014; Mica Lake, Schiff et al., 2009). However, except for the common change between mid- and late Holocene observed at multiple locations, the $\delta^{18}O$ records show large spatiotemporal variability across mainland Alaska, the northern Gulf of Alaska, and the contiguous United States. Such heterogeneous trends could be explained by the complex patterns of precipitation $\delta^{18}O$ anomalies associated with AL behavior (Berkelhammer et al., 2012), which are also complicated by both changes in intensity and spatial position changes (e.g., Rodionov et al., 2005; Sugimoto and Hanawa, 2009). Furthermore, large age uncertainties of sedimentary records and a variety of other local influences on $\delta^{18}O$ values including topography, temperature, and effective moisture (precipitation minus evaporation) could further contribute to spatiotemporal differences in paleoclimatic $\delta^{18}O$ variability (e.g., Anderson et al., 2016). These differences between $\delta^{18}O$ records have caused considerable difficulties in reconstructing consistent long records of AL variability (Newman et al., 2016).

The climate mechanism(s) that are responsible for generating AL changes over recent instrumental timescales are also poorly understood. One important component is the Westerly Jet (WJ), which flows at an altitude of approximately 9–16 km above sea level and circles the globe along a meandering path, and which is closely associated with hemispheric-scale climate changes. Recent meteorological records indicate that the AL is sensitive to the dynamics of the WJ over East Asia and the North Pacific Ocean, with impacts observed on cyclogenesis, monsoon development, and storm tracks (e.g., White and Barnett, 1972; Lau, 1988; Dole and Black, 1990; Nakamura et al., 2002; Yang et al., 2002; Athanasiadis et al., 2010; Park and An, 2014). However, at timescales that exceed the recent instrumental record, the interactions between the AL and the WJ are virtually unknown.

The limited paleoclimatic history of the AL and its interactions with other components of the climate system indicate these high-priority questions remain to be answered:

- What is the timing and nature (intensity and/or position) of AL variability during the Holocene?
- Is there evidence of linkages between the AL and WJ at centennial and longer timescales?
- What are the external drivers of AL variability?

The present study was designed to address these questions by (i) conducting multivariate principal component analysis (PCA) using published $\delta^{18}O$ records from Alaska, northwestern Canada, and the western United States to eliminate local environmental effects on each $\delta^{18}O$ record; (ii) identifying

https://doi.org/10.1017/qua.2020.116 Published online by Cambridge University Press

common pattern(s) of $\delta^{18}O$ anomalies across such areas since 7.5 ka, and trace multi-centennial and longer AL variations; (iii) compare the reconstructed AL variations with records of the WJ in East Asia and the western North Pacific Ocean to determine linkages; and (iv) use these combined AL and WJ datasets to better clarify dynamic changes in North Pacific atmospheric circulation and elucidate the potential triggers of Holocene climate variability.

DATA USED FOR PRINCIPAL COMPONENT ANALYSIS

Many $\delta^{18}O$ profiles covering part or all of the Holocene have been reported from Alaska, Canada, and the central and northwestern United States. These include $\delta^{18}O$ of calcite or opal in lake sediments (e.g., Anderson et al., 2005; Schiff et al., 2009; Clegg and Hu, 2010; Anderson, 2011, 2012; Steinman and Abbott, 2013; Wooller et al., 2012; Yuan et al., 2013), organic matter in peat (Jones et al., 2014), ice (Fisher et al., 2008), and speleothem carbonate (Ersek et al., 2012). For this analysis, paleoclimatic $\delta^{18}O$ records with sample resolution exceeding one data point every 250 years and durations that include the last 7.5 ka were selected for PCA.

A key second requirement for the PCA input dataset was that records are more sensitive to precipitation $\delta^{18}O$ and had minimal evaporation-caused fractionation effects. Anderson et al. (2016) compiled lake water $\delta^{18}O$ and $\delta^{2}H$ values from western North America and identified eight spatial groups (Colorado/Utah, eastern Washington, Montana/Idaho/Wyoming, British Columbia/Alberta, Yukon Territory, Alaska-central interior, Alaska-Brooks Range, and Alaska-northeast interior) using an analysis of regional evaporation water lines and the Global Meteoric Water Line (fig. 2 in Anderson et al., 2016). The record from each regional group that showed the smallest influence from evaporative effects, as well as met the requirements for sample resolution and duration, was selected for further analysis.

Seven $\delta^{18}O$ records met the above criteria (Table 1, Fig. 1), including: 1) sedimentary calcite from Takahula Lake, south-central Brooks Range, Alaska (Clegg and Hu, 2010); 2) Mt. Logan ice core, northwestern Canada (Fisher et al., 2008; Osterberg et al., 2014, 2017); 3) sedimentary calcite from Jellybean Lake, Yukon Territory, Canada (Anderson et al., 2005); 4) sedimentary calcite from Paradise Lake, central British Columbia (Steinman et al., 2016); 5) sedimentary calcite from Lime Lake, eastern Washington (Steinman et al., 2016); 6) sedimentary calcite from Bison Lake, Central Rocky Mountains, central United States (Anderson, 2011), and; 7) a speleothem deposit from Oregon Caves National Monument (OCNM) in southwestern Oregon, western United States (Ersek et al., 2012).

Each of these $\delta^{18}O$ records was examined in terms of a combination of hydrological settings, relationship between lake water $\delta^{18}O$ and $\delta^{2}H$, and its seasonality changes (Anderson et al., 2005; Clegg and Hu, 2010; Anderson, 2011; Steinman et al., 2016), meteorological data (Fisher et al., 2008; Ersek et al., 2012), and lake hydrologic and/or isotope mass balance modeling (Steinman et al., 2016). The records from Takahula and Paradise Lakes are characterized by closed-basin isotope systems, and are reported to be influenced by many factors such as effective moisture, temperature, source area of moisture (e.g., atmospheric circulation patterns), precipitation amount and seasonality (Clegg and Hu, 2010; Steinman et al., 2016). In contrast, the $\delta^{18}O$ record from Jellybean Lake (an open-basin system) was originally thought to result from isotope fractionation during moisture transport from the Gulf of Alaska across the St. Elias Mountains that reflected atmospheric circulation patterns (Anderson et al., 2005). However, Anderson et al. (2016) revised their original interpretation to moisture source change because the relationship between $\delta^{18}O$ of Jellybean Lake and NPI was oppositely reported in Anderson et al. (2005).

Similarly, records from open-basin Lime and Bison Lakes were interpreted as being influenced by precipitation $\delta^{18}O$ values that reflect atmospheric circulation patterns and seasonality of precipitation (Steinman et al., 2016; Anderson, 2011). The dominant signal in the $\delta^{18}O$ record from Mt. Logan is thought to represent source area of moisture (Fisher et al., 2008; Osterberg et al., 2014, 2017), while the OCNM speleothem $\delta^{18}O$ data mainly represents temperature (Ersek et al., 2012).

METHODOLOGY

Principal Component Analysis

Principal Component Analysis (PCA) reduces the complexity of multivariate data into a few interpretable directions of variability, or principal components, that represent synthetic variables and explain cumulative independent proportions of variance within the raw data (ter Braak and Prentice, 1988). PCA (also known as Empirical Orthogonal Function analysis [EOF]) has been applied to modern climatology, oceanography, and paleoclimatology variables to extract climate dynamics behind the spatial distribution of observational/proxy datasets (e.g., Mantua et al., 1997; Thompson and Wallace, 1998; Kaplan and Wolfe, 2006; Harada et al., 2012). In this study, we conducted PCA to empirically find common $\delta^{18}O$ patterns of variability among stations selected from a wide geographic area in western North America. Since each $\delta^{18}O$ record should be regarded as a superposition of both regional and local components, PCA can be useful for extracting regional components from these multiple $\delta^{18}O$ records. Because AL intensity and position largely determine precipitation $\delta^{18}O$ values and winter precipitation amounts over western North America (Berkelhammer et al., 2012; Liu et al., 2014), comparisons between the spatial loading patterns of each Principal Component (PC) and (i) the winter precipitation amount from reanalysis datasets (NOAA-20C reanalysis, Compo et al., 2011; NCEP II Reanalysis, Kanamitsu et al., 2002) and (ii) the simulated $\delta^{18}O$ anomalies using IsoGSM (Yoshimura et al., 2008; Berkelhammer

https://doi.org/10.1017/qua.2020.116 Published online by Cambridge University Press

Table 1. Western North America paleoclimate $\delta^{18}O$ proxy records used in this study.

No.*	Site name	Region	Basin system	Material	Lat	Long	Elevation (m asl)	Age constraint	Duration and resolution (years: average, lowest)	Main interpretation of $\delta^{18}O$ variation by original authors	References
1	Takahula Lake	South-central Brooks Range	Closed	Calcite	67.35°N	153.66°W	275	^{14}C, ^{210}Pb	8200 years (65, 238)	Evaporation, amount of winter precipitation	Clegg and Hu, 2010
2	PRCol, Mt. Logan	Yukon Territory	-	Ice	60.60°N	140.50°W	5340	Annual layer counting (last 300 years), theoretical model	12,000 years (25, 59)	Moisture source	Fisher et al., 2008
3	Jellybean Lake	Yukon Territory	Open	Calcite	60.35°N	134.80°W	730	^{14}C, ^{210}Pb, ^{137}Cs, volcanic event	7600 years (22, 68)	Moisture transport path, moisture source	Anderson et al., 2005, 2016
4	Paradise Lake	Central British Columbia	Closed	Calcite	54.69°N	122.62°W	733	^{14}C, ^{210}Pb	9100 years (20, 178)	Evaporation, amount of winter precipitation	Steinman et al., 2016
5	Lime Lake	Eastern Washington	Open	Calcite	48.87°N	117.34°W	781	^{14}C, ^{210}Pb, volcanic events	7800 years (33, 169)	Temperature, amount of winter precipitation, moisture source	Steinman et al., 2016
6	Oregon Caves National Monument (OCNM)	Southwestern Oregon	-	Speleothem	42.08°N	123.42°W	1200	U-Th	8000 years (3, 50)	Temperature	Ersek et al., 2012
7	Bison Lake	Central Rocky Mountains	Open	Calcite	39.77°N	107.35°W	3255	^{14}C	10,300 years (30,89)	Moisture source, precipitation seasonality	Anderson, 2011

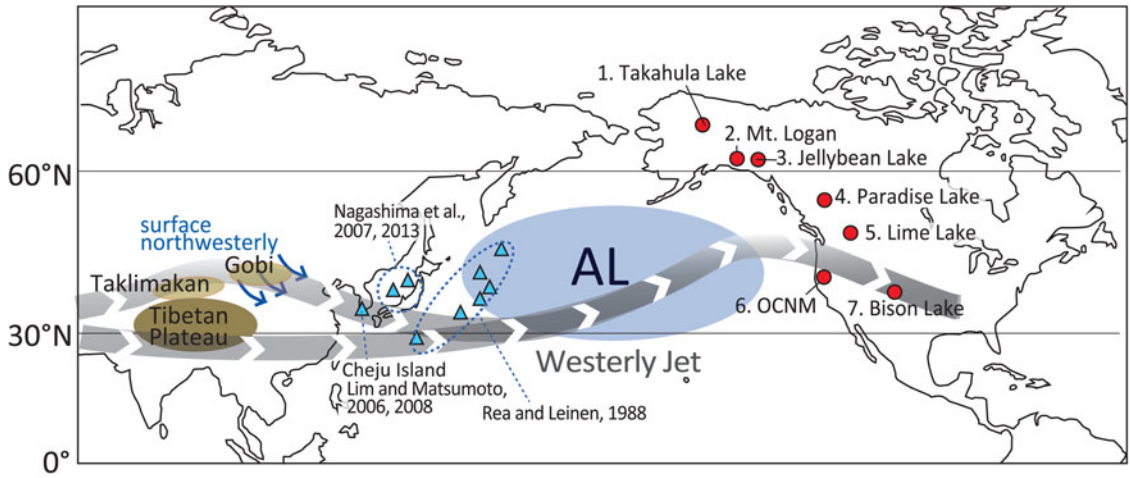

Figure 1. Schematic of North Pacific winter atmospheric circulation patterns and location of sites with $\delta^{18}O$ records used in this study for Aleutian Low (AL; red circles) and Westerly Jet (WJ; blue triangles) reconstructions. The number adjacent to each red circle corresponds to the site number in Table 1.

et al., 2012; Yoshimura, 2015) are useful for evaluating possible AL relationships with each calculated PC.

PCA was applied to the seven $\delta^{18}O$ profiles for the time range of 7.5–0.4 ka, after 1) calculating mean $\delta^{18}O$ values at 50-yr time steps for each record after considering age uncertainties (see the following subsection) and 2) standardizing to a mean of 0 and a standard deviation of 1. The resultant PCA had two components with eigenvalues that exceeded 1.0, which together account for 68% variance explained in the underlying data (Supplementary Figure 1a). When examining the extracted communalities (e.g., the variance in each dataset that is explained by the PCA method; Supplementary Figure 1b), the median value of 69% demonstrates that PCA is a good descriptor of the combined $\delta^{18}O$ dataset. This is further confirmed by a Kaiser-Meyer-Olkin value of 0.620, which indicates that some of the underlying variance among datasets may be explained by common variance; values greater than 0.6 are considered adequate for PCA (Kaiser, 1974; Cerny and Kaiser, 1977). Finally, the PCA analysis also exceeded a significance test of <0.0001 for the Bartlett's Test of Sphericity, which tests if the PCA correlation matrix is different from an identity matrix; this result signifies there are related features in the source data that can be described by PCA. Taken together, these diagnostic analyses show that the selected $\delta^{18}O$ records have shared underlying properties that are appropriate for examination using the PCA method.

Method for $\delta^{18}O$ smoothing based on age uncertainties

To apply the PCA method to paleoclimate proxy records that have independent age models, a new technique that averages the raw data of selected sample intervals with respect to age uncertainties was developed. First, age uncertainties (1σ) were calculated by a Bayesian age-depth model using OxCal software 4.3.2 (Bronk Ramsey, 2009; https://c14.arch.ox.ac.uk/oxcal.html). The model used the age datums reported in each original reference, such as ^{14}C, ^{210}Pb, and U-Th ages (Table 1, Supplementary Figure 2). The age uncertainties compared against sample depths indicate the statistically possible range of sample depths that correspond with each age, as is schematically shown for the Bison Lake age-depth model example in Figure 2. Through averaging the $\delta^{18}O$ value within the corresponding depth interval for each age, we could eliminate any possible biases on PCA originated from uncertainty in the correlation of isotope variations among sites (Fig. 3). This averaging process was conducted for the $\delta^{18}O$ profile with linear interpolation at 0.03 mm depth intervals for OCNM and 0.1 cm depth intervals for the remaining records.

The age model for the Mt. Logan ice core is excluded from the preceding Bayesian treatment, as it was constructed using annual layer counting for the last 300 years and a theoretical accumulation model that placed a clear transition in electrical conductivity at 11.7 ka, based on a similar transition seen in Greenland (Fisher et al., 2008). Instead, the $\delta^{18}O$ averaging was conducted using original age uncertainties determined by the authors (Fisher et al., 2008; ages younger than 0.3 ka ± 2 years, 0.6–0.3 ka ± 5%, and 4–0.6 ka ± 15%) and assuming a more conservative ± 20% between 7.5–4 ka as the age uncertainty for this time interval was not originally described. The averaging process between 6.3–0.4 ka was applied to the $\delta^{18}O$ profile with linear interpolation at 0.1 m depth intervals, and for the portions of the Mt. Logan core that predate 6.3 ka, the original $\delta^{18}O$ time intervals without linear interpolation were used because of pre-existing depth uncertainties (and accompanying time uncertainty) associated with the lower part of the core (Osterberg, E., personal communication, 2020). Finally, the temporal record of

https://doi.org/10.1017/qua.2020.116 Published online by Cambridge University Press

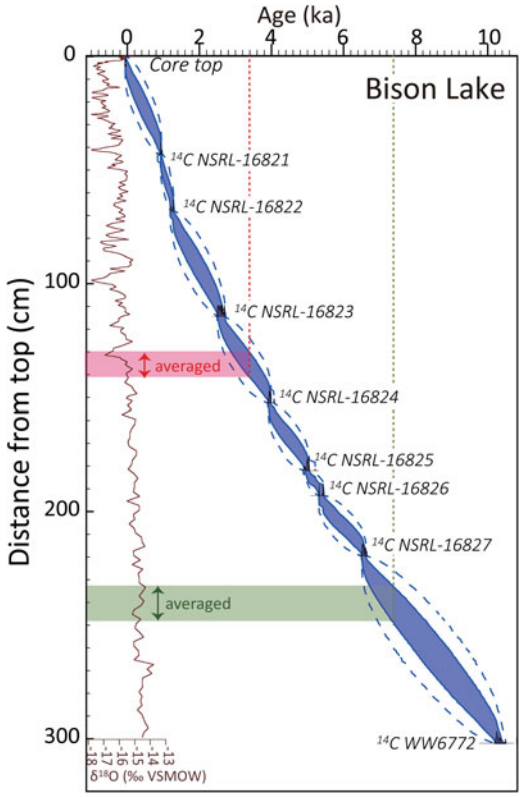

Figure 2. A schematic example showing the $\delta^{18}O$ smoothing method based on age uncertainties estimated by a Bayesian approach (Bronk Ramsey, 2009) for the case of Bison Lake (Anderson, 2011). Shaded blue area and dotted blue lines indicate the modeled error envelope at 1σ and 2σ levels, respectively. Shaded red and green areas show depth intervals of averaged $\delta^{18}O$ data for two example time periods at 3.4 and 7.4 ka, respectively.

averaged $\delta^{18}O$ was extracted with 50-yr time steps for each site and used for PCA.

RESULTS AND DISCUSSION

The $\delta^{18}O$ records from western North America and results of Principal Component Analysis

The seven western North America $\delta^{18}O$ records are spread across a large distance but nonetheless share several common features at millennial and longer timescales (Fig. 3). The $\delta^{18}O$ records from Mt. Logan (Fig. 3b) and Jellybean Lake (Fig. 3c) show a similar pattern with local $\delta^{18}O$ maxima at ~6 and 2–1.5 ka, and local minima between 4.5–4 and 1.2–0.5 ka. This $\delta^{18}O$ pattern is generally opposite to results from Takahula Lake (Fig. 3a). These millennial-scale $\delta^{18}O$ trends are not clearly recorded in records from central and western United States. Instead, the $\delta^{18}O$ records from Paradise and Lime Lakes, and OCNM, show an increasing trend from the mid- to late Holocene punctuated with millennial-scale oscillations, while the $\delta^{18}O$ record from Bison Lake is characterized by a semi-continuous decreasing trend from the mid- to late Holocene (Figs. 3d–g).

The different time-scale trends observed qualitatively from the seven $\delta^{18}O$ records are further clarified by PCA. The first principal component (PC1) explains 42% of the variance, and has a temporal pattern that is characterized by a continuous increasing trend with negative values between 7.5–3.9 ka and positive values at 3.9–0.4 ka (Fig. 4a). Specific datasets associated with strong positive loadings for PC1 are observed at Paradise and Lime Lakes, and OCNM in the western United States, while strong negative loading is observed at Bison Lake (Fig. 4c). In addition, weak positive loadings are observed at Jellybean and Takahula Lakes. PC2 describes 24% of the data variance and is characterized by multi-centennial to millennial-scale trends with positive PC2 scores occurring at 7.5–5.1, 2.4–1.2, and 0.7–0.4 ka (Fig. 4b). Strong positive PC2 loadings are observed at Mt. Logan, Jellybean and Lime Lakes, while strong negative loadings are seen at Takahula Lake (Fig. 4d).

Principal Components and Aleutian Low variations

First Principal Component

The PC1 explains high variance (42%) and is dominated by high loading values observed across western North America. This common $\delta^{18}O$ pattern among stations spread across western North America suggests local effects are likely not responsible for the similarities in $\delta^{18}O$ variability reflected in PC1. The wide distribution of these associated sites suggests atmospheric circulation changes, including the AL system, have high potential to generate these similar $\delta^{18}O$ changes (Berkelhammer et al., 2012; Liu et al., 2014).

Placing the PCA loading results of the $\delta^{18}O$ proxy data into a spatial context, the distribution of PC1 loading scores corresponds largely with the pattern of simulated $\delta^{18}O$ anomalies that are associated with the PNA teleconnection pattern (Fig. 5a). The PNA simulation using IsoGSM reveals a positive anomaly (1–2‰) of precipitation $\delta^{18}O$ in the winter season (December–March) over the northern to northwestern United States of ca. 40–70°N and 90–130°W in contrast to the strong negative anomaly over the southern to southeastern United States during PNA positive years (Liu et al., 2014). These spatial features could be explained by the characteristic positive PNA atmospheric circulation pattern, where stronger AL and high pressure over the intermontane region of North America generate increased moisture transport from $\delta^{18}O$ enriched tropical oceans to the northwestern United States, while $\delta^{18}O$ depleted moisture accumulates in the southeast United States (Fig. 5a). The prominent positive $\delta^{18}O$ anomalies in western North America represented by Paradise Lake, Lime Lake, and OCNM, and the negative $\delta^{18}O$ anomaly at southernmost site of Bison Lake associated with the positive PC1 score at 3.9–0.4 ka show a good similarity with the characteristic northwestern enriched-southeastern depleted $\delta^{18}O$ pattern of winter precipitation caused by the PNA positive state.

https://doi.org/10.1017/qua.2020.116 Published online by Cambridge University Press

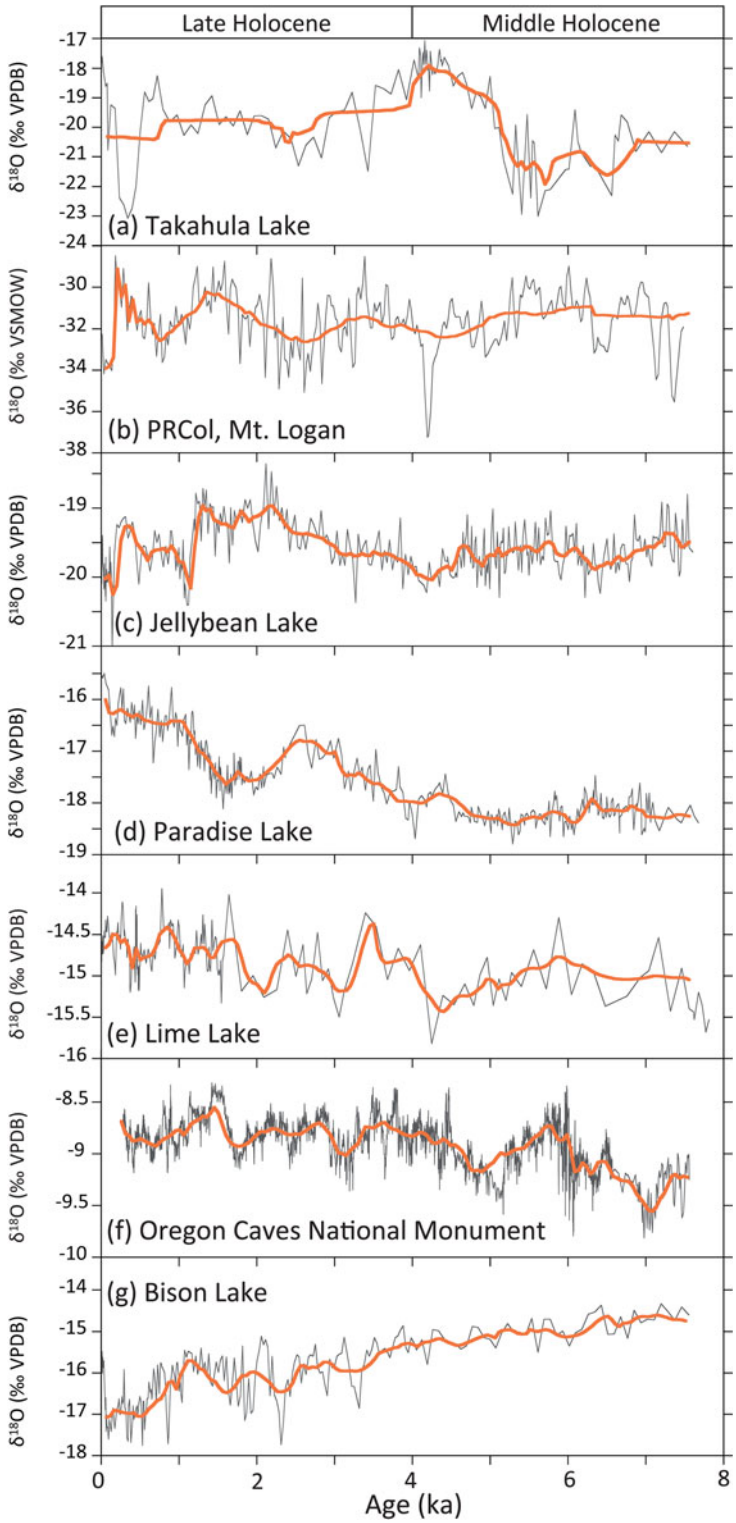

Figure 3. Millennial-scale comparison of $\delta^{18}O$ records used in the PCA: (a) sedimentary calcite from Takahula Lake, Alaska (Clegg and Hu, 2010); (b) Mt. Logan ice core, northwestern Canada (Fisher et al., 2008; Osterberg et al., 2014, 2017); (c) sedimentary calcite from Jellybean Lake, Yukon Territory (Anderson et al., 2005); (d) sedimentary calcite from Paradise Lake, Central British Columbia (Steinman et al., 2016); (e) sedimentary calcite from Lime Lake, Eastern Washington (Steinman et al., 2016); (f) speleothem from Oregon Caves National Monuments (OCNM), western United States (Ersek et al., 2012); and (g) sedimentary calcite from Bison Lake, central United States (Anderson, 2011). Dark gray lines show raw data and thick orange lines show $\delta^{18}O$ values averaged for the depth intervals determined by age uncertainties.

https://doi.org/10.1017/qua.2020.116 Published online by Cambridge University Press

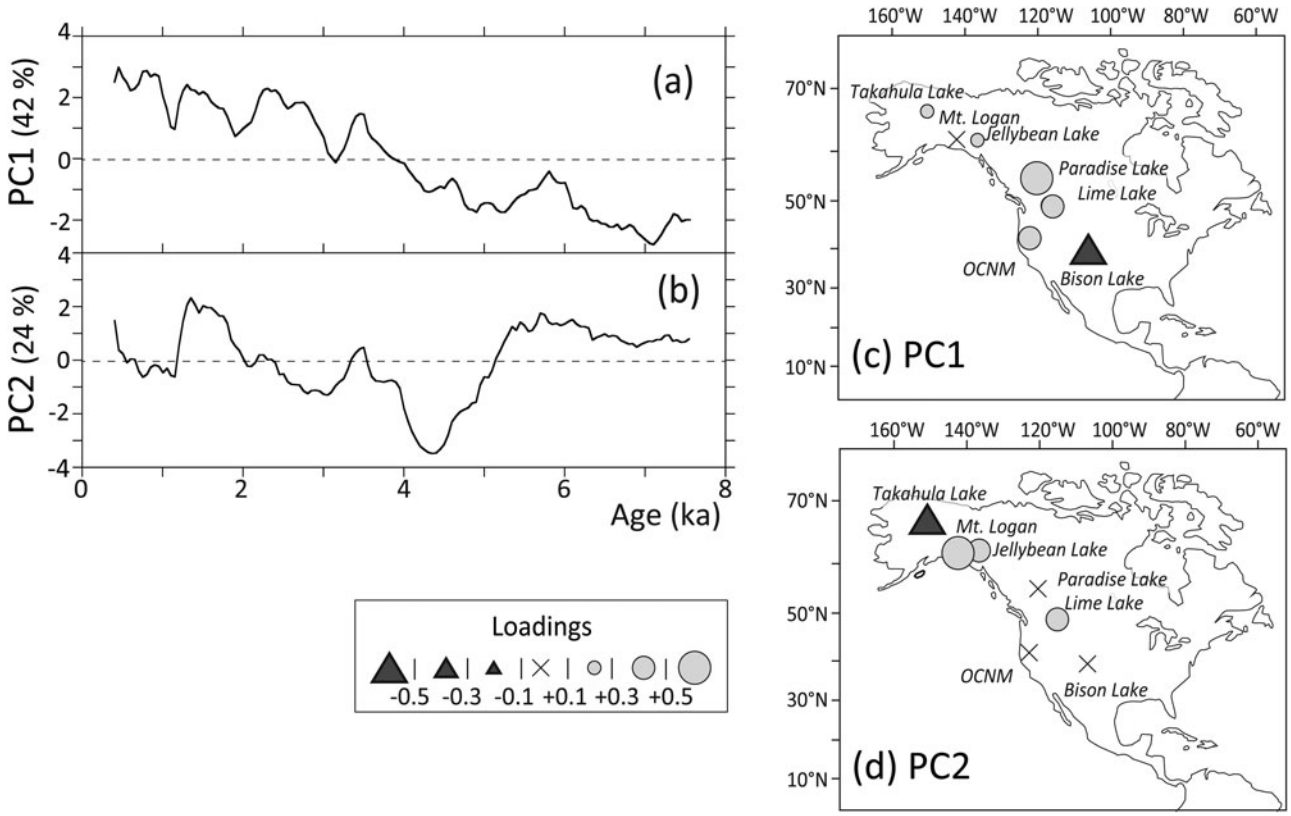

Figure 4. Principal Component Analysis (PCA) of $\delta^{18}O$ records since 7.5 ka: (a) first principal component (PC1); (b) second principal component (PC2); (c) and (d) spatial distribution of $\delta^{18}O$ records with loading scores corresponding to PC1 and PC2, respectively.

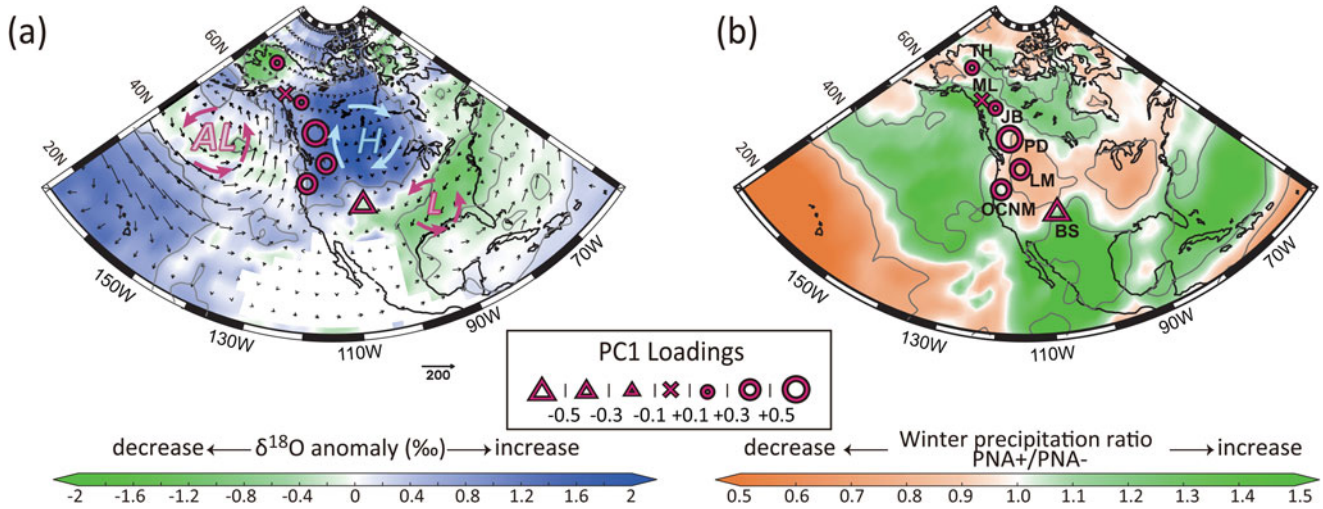

Figure 5. PC1 loadings compared to the (a) simulated winter (DJFM) precipitation $\delta^{18}O$ and vertically integrated moisture flux (arrows; kg m^{-1} s^{-1}) differences between PNA positive (PNA index > 0.5; n = 17) and negative (PNA index < 0.5: n = 14) years for AD 1950–2005 (PNA positive-PNA negative) using the Twentieth Century Isotope Reanalysis (IsoGSM20C, Yoshimura, 2015) after the method of Liu et al. (2014), (b) winter precipitation ratio between the PNA positive and negative years (amount of winter precipitation averaged for PNA positive years divided by that for PNA negative years) from NOAA-20C reanalysis (Compo et al., 2011). The areas enclosed by the grey lines in (a) and (b) show significance at the P < 0.1 level for $\delta^{18}O$ and winter precipitation differences between PNA positive and negative years, respectively. TH: Takahula Lake, ML: Mt. Logan, JB: Jellybean Lake, PD: Paradise Lake, LM: Lime Lake, OCNM: Oregon Caves National Monument, BS: Bison Lake.

https://doi.org/10.1017/qua.2020.116 Published online by Cambridge University Press

Since the PNA also generates large shifts in winter precipitation amounts across wide areas of North America (Liu et al., 2017), further examination of precipitation seasonality is needed to test possible connections between PNA and the $\delta^{18}O$ anomalies attributed to PC1. Precipitation $\delta^{18}O$ tends to be depleted in winter compared to summer throughout western to northwestern North America (Vachon et al., 2007), hence abundance (less abundance) of winter precipitation compared to summer precipitation generates depletion (enrichment) of the total precipitation $\delta^{18}O$. The resulting spatial pattern of winter precipitation differences between the PNA positive (n = 17) and negative (n = 14) years for the period AD 1950–2005 (NOAA-20C reanalysis; Compo et al., 2011) shows significant winter precipitation increase along the Pacific coast of North America, Mexico, and the far northern reaches of Canada and Alaska, while precipitation decreases are observed in the continental interior of North America (Fig. 5b). The winter precipitation decreases in the North America interior, and the increases in Central America, enhance the trend of enriched and depleted $\delta^{18}O$ in winter precipitation of the two areas, respectively, during positive PNA patterns (Fig. 5). Therefore, the changes in winter precipitation $\delta^{18}O$ and amounts responding to a positive PNA together generate the higher loading scores at Paradise, Lime, and Bison Lakes, and OCNM. In contrast, winter precipitation increases around the coastal Gulf of Alaska, and decreases in the Alaskan interior tend to cancel the enriched and depleted $\delta^{18}O$ anomalies in winter precipitation of each area, which may explain the lower PCA loading scores associated with Takahula Lake, Jellybean Lake, and Mt. Logan. Together, these observations suggest $\delta^{18}O$ changes represented by PC1 can be explained by PNA-like state changes, with positive PC1 values during the late Holocene corresponding to PNA positive state.

Regional-scale temperature changes may be an alternative explanation to generating the $\delta^{18}O$ variabilities reflected in PC1, as was originally suggested for the Lime Lake and OCNM sites (Table 1, Ersek et al., 2012; Steinman et al., 2016). However, recently published temperature reconstructions using macrofossil communities in western North America (Harbert and Nixon, 2018) and compiled pollen and other proxies in central North America (Shuman and Marsicek, 2016) do not support this possibility. According to Harbert and Nixon (2018), reconstructed temperatures at western North America show higher than present temperatures both in winter and summer throughout the mid- to late Holocene with millennial scale minimum between ca. 5–3 ka. This warming trend seems unlikely to explain the prominent $\delta^{18}O$ changes observed during this period. Similarly, the temperature reconstructed by pollen and other proxies shows no prominent change between the mid- and late Holocene (Shuman and Marsicek, 2016).

Second Principal Component

In contrast to PC1, higher loading scores for PC2 are mainly observed along the northern Gulf of Alaska (Fig. 4d). The $\delta^{18}O$ variability reflected in PC2 is observed from the lake records of both closed-basin (Takahula Lake) and open-basin (Jellybean Lake) systems, and from the Mt. Logan ice core record with extreme topography that exceeds an elevation of 5000 m. This variability of settings for these $\delta^{18}O$ archives most closely associated with PC2 suggests that dynamic atmospheric circulation changes may be responsible for PC2 rather than local forcing.

According to Berkelhammer et al. (2012), a typical strengthened/westward-shifted AL (such as observed during the winter of AD 2003) generates increased moisture transport from $\delta^{18}O$ enriched tropical oceans to western North America and coastal Alaska, along with cyclonic wind anomalies (Figs. 6c, 6f). Under this configuration, the most prominent $\delta^{18}O$ enrichment is observed over the Pacific margin of North America rather than the western interior United States, due to the more westerly position of the AL (Fig. 6f). This spatial pattern of $\delta^{18}O$ anomalies contrasts sharply with the patterns associated with strengthened and eastward-shifted AL conditions, or weakened AL conditions, as typically seen during the winters of AD 1998 and 1989, respectively (Figs. 6d–e). The location of records with high PC2 loading scores (the Mt. Logan, Jellybean Lake, and Lime Lake records) within this zone of enriched $\delta^{18}O$ suggests they would be consistent with strengthened and westward-shifted AL regimes.

The remaining $\delta^{18}O$ records from inland Alaska and western North America are located in areas with either prominent $\delta^{18}O$ enrichment (OCNM) or no substantial $\delta^{18}O$ anomalies (Takahula Lake, Paradise Lake, and Bison Lake) (Fig. 6f). However, these sites may be consistent with the combination of winter precipitation changes associated with a strengthened and westward-shifted AL system (Figs. 6f–g). The NCEP II Reanalysis data for the AD 2003 pattern shows an extreme winter precipitation increase over Alaska, while winter precipitation anomalies elsewhere are relatively small and show a mosaic pattern around western and northern North America (Fig. 6g). These AL-driven large changes in winter precipitation for Alaska have also been reported from the long-term (AD 1951–2005) observation record of Clegg and Hu (2010). The amount of winter (December–March) precipitation at the Bettles weather station near Takahula Lake shows ca. 70% increase in AD 2003 compared to the average winter precipitation for AD 1952–2020 (Western Regional Climate Center; https://wrcc.dri.edu/). Since winter precipitation at Takahula Lake is highly depleted $\delta^{18}O$ (modeled value of -24‰) in contrast to the enriched $\delta^{18}O$ (modeled value of -14‰) of summer precipitation (Clegg and Hu, 2010), this large increase in winter precipitation likely generates the $\delta^{18}O$ depletion. Similarly, slight increase of winter precipitation around OCNM generates $\delta^{18}O$ depletion, compensating the enriched $\delta^{18}O$ in winter precipitation of this area. The remaining two stations of Paradise Lake and Bison Lake are located around the boundaries between the negative and positive anomalies for both amount of the winter precipitation and the $\delta^{18}O$ (Figs. 6f–g), which likely explains their low PC2 loading scores.

An alternative explanation for PC2 is temperature change, as was originally interpreted for Lime Lake in the Pacific

https://doi.org/10.1017/qua.2020.116 Published online by Cambridge University Press

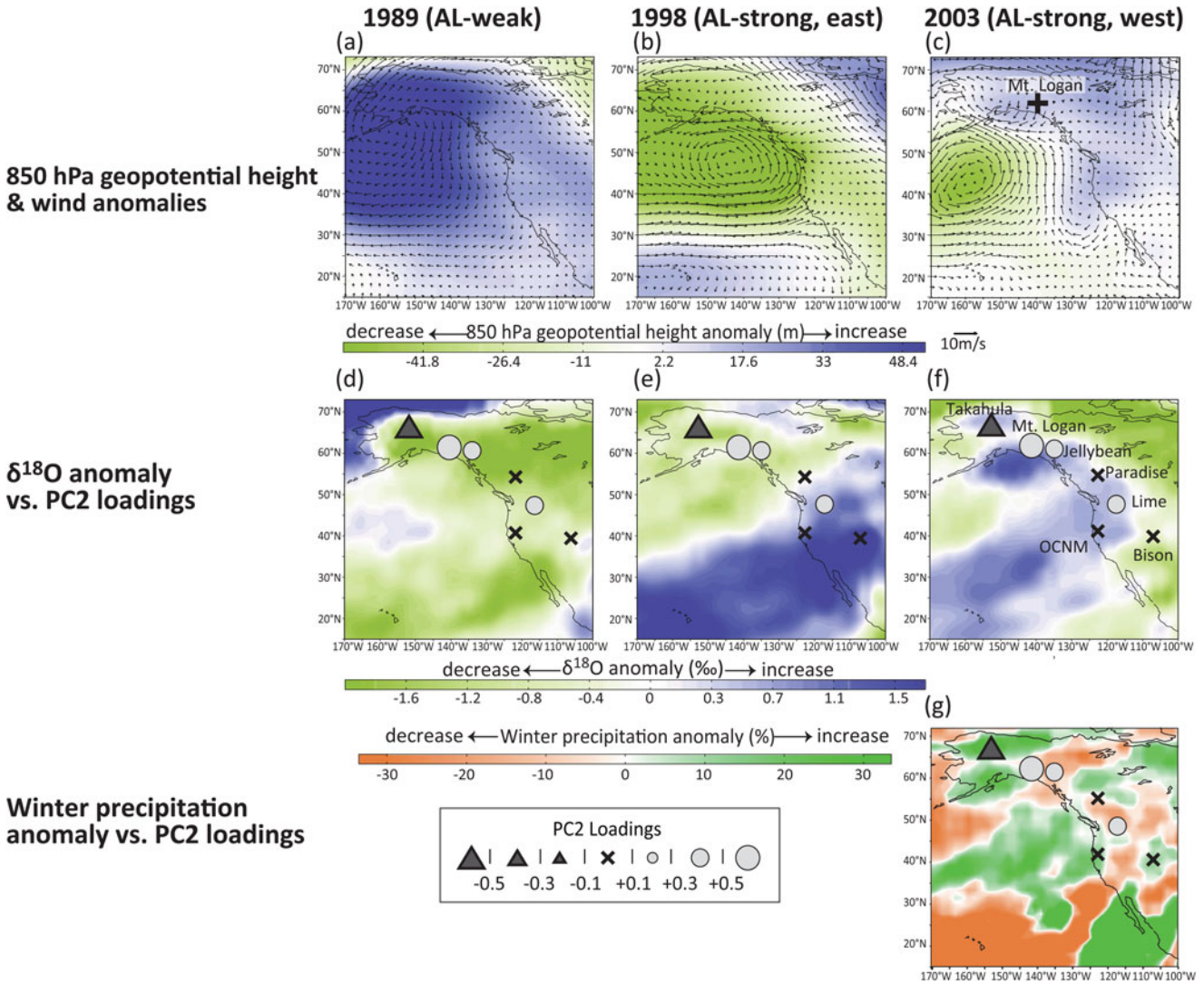

Figure 6. Comparison of PC2 spatial loading patterns and simulated precipitation $\delta^{18}O$ anomalies during the winters (NDJFM) of AD 1989 (weak AL), AD 1998 (strong and east AL) and AD 2003 (strong and west AL) after Berkelhammer et al. (2012), and AD 2003 winter precipitation anomalies. Average annual 850 hPa geopotential height (m) and wind vector anomalies (m/s) from NCEP II Reanalysis (Kanamitsu et al., 2002) during AD 1989, 1998 and 2003 (a–c), the $\delta^{18}O$ anomalies in winter precipitation from IsoGSM associated with these same years (Berkelhammer et al., 2012) (d–f) and winter precipitation anomalies of AD 2003 from NCEP II Reanalysis (g) plotted with the loadings of PC2.

Northwest (Steinman et al., 2016). A quantitative temperature reconstruction study using the modern analogue technique for pollen from the northern Gulf of Alaska and the Alaskan interior (which contain $\delta^{18}O$ records with high PC2 loading scores) shows slightly higher winter/annual temperatures during the mid-Holocene that gradually decrease to the present (Viau et al., 2008). For summer temperatures, this reconstruction shows almost constant values for both the mid- and late Holocene, as well as a lack of millennial-scale temperature changes (Viau et al., 2008). Other temperature records for this same area derived from midges, pollen, and biogeochemical indicators show gradual temperature decrease from mid-Holocene toward the present, with slight millennial-scale maxima around 3–2 ka and minima around 2–1 ka (Kaufman et al., 2016). These studies thus cannot account for the higher $\delta^{18}O$ anomalies seen around the Gulf of Alaska during 2–1 ka, which are described by a positive PC2 score (Fig. 4b).

In summary, PC1 and PC2 that were extracted by multivariate PCA statistical methods applied to these paleoclimate proxy $\delta^{18}O$ records appear to reflect different states of AL changes and atmospheric modes. The former reflects negative to positive PNA-like state changes characterized by AL intensification from mid- to late Holocene, which is consistent with previous work by Liu et al. (2014). In contrast, PC2 reflects centennial to millennial-scale changes in AL intensity and longitudinal position. It should be noted that the temporal variation of PC2 shows close similarity to the stacked $\delta^{18}O$ records from Mt. Logan ice, Jellybean and Mica Lakes, and Horse Trail Fen (Kaufman et al., 2016), even though the latter two records were excluded from the PCA dataset due to lower

https://doi.org/10.1017/qua.2020.116 Published online by Cambridge University Press

time resolutions (Jones et al., 2014; Schiff et al., 2009). Nevertheless, this similarity supports the idea that the $\delta^{18}O$ variability reflected in PC2 is the typical $\delta^{18}O$ feature of paleo-archives from the northern Gulf of Alaska because both the amount of winter precipitation and the regional $\delta^{18}O$ values of this area seem to be sensitive to AL spatial changes.

The interpretations that $\delta^{18}O$ changes represented by PC1 and PC2 reflect changes in winter precipitation amount and $\delta^{18}O$ values are basically consistent with the original interpretations of these datasets (Table 1). The exception is the record from OCNM, where the investigators interpreted that temperature is the dominant factor controlling $\delta^{18}O$ values, based on a significant correlation ($r^2 = 0.65$) between amount-weighted monthly precipitation $\delta^{18}O$ values and monthly temperature at the location (Ersek et al., 2010, 2012). However, this high correlation between monthly averaged $\delta^{18}O$ and temperature does not necessarily explain longer-timescale precipitation $\delta^{18}O$ changes since it is based on three years observations. Hence it cannot easily be dismissed that winter precipitation amount and $\delta^{18}O$ changes forced by paleoclimatic AL dynamic shifts have not played a significant role in the $\delta^{18}O$ changes recorded at OCNM.

Comparison to other Aleutian Low records

Comparing the $\delta^{18}O$ PCA results with other records of past AL variability places these findings into a broader context. The sodium concentration record of the Mt. Logan ice core (Fig. 7f; Fisher et al., 2008; Osterberg et al., 2014, 2017) shows poor resemblance to the temporal profile of PC1, but shows good agreement with PC2, where higher sodium concentrations correspond with lower PC2 values (Figs. 7a, 7e–f; note the Y-axis of Fig. 7e is reversed). However, the previously offered explanations for these two records are inconsistent. The positive PC2 record suggests a strengthened and westward-shifted AL, while low sodium concentration record suggests a weakened AL. This discrepancy could be attributed to the large influence that AL location has on sea salt transport to Mt. Logan. When the AL shifts westward, southerly winds intensify over the eastern North Pacific Ocean (Fig. 6c), and the region that is located between a zone of lower 850 hPa geopotential height anomaly in the west and a higher anomaly zone in the east also shifts westward (Berkelhammer et al., 2012). These movements result in a northerly wind anomaly over Mt. Logan (Fig. 6c) that might limit sea salt transport along coastal areas despite strengthened AL intensity. This potential influence of AL position change on sodium concentration in the Mt. Logan ice-core record may also explain the somewhat weak correlation ($r = -0.45$) observed between the sodium concentration and the December-March AL intensity record between AD 1990–1998 (Osterberg et al., 2014). Furthermore, Mt. Logan sodium concentrations show decadal-scale decreases during ca. AD 1930–1940 when an intensified AL was observed (Anderson et al., 2016). This discrepancy could also be attributed to a westward shift of the AL observed during the same period (Overland et al., 1999).

A 2000-year moving window cross-correlation calculated between the Mt. Logan sodium record and PC2 shows that the correlation between these datasets is negative between ca. 6–2 ka and positive after 2 ka (Fig. 7g; note the Y-axis is reversed)). Between 2–1.1 ka and after ca. 0.5 ka, PC2 increases with the increase of sodium concentrations at Mt. Logan, and both trends are inversed during 1.1–0.5 ka. The increase in PC2 and increase in sodium concentration at 2–1.1 ka and after 0.5 ka is consistent with the previous suggestion of a strengthened AL with a westward shifted center. During these periods, the extent of the AL westward shift may be small enough so as to not limit sea salt transport to Mt. Logan by the northerly wind anomaly pattern. This comparison between the $\delta^{18}O$ PC2 composite and the Mt. Logan sodium record highlights the difficulties of estimating both intensity and position change of the AL using single station paleoclimate records.

The late Holocene negative PC2 scores and lower sodium concentrations at Mt. Logan (Osterberg et al., 2014) consistently suggest weaker AL at ca. 1.2–0.6 ka (1.1–0.7 ka at Mt. Logan), an interval broadly consistent with the Medieval Warm Period. A weakening of the AL during the Medieval Warm Period is consistent with a reconstruction of the Pacific Decadal Oscillation (PDO) index, where a negative PDO shift is interpreted from hydrologically sensitive tree-ring records in southern California and western Canada (MacDonald and Case, 2005). At the same time, greater aridity across the western United States is seen in a compilation of drought sensitive tree-ring records (Cook et al., 2004), and while there are complex reasons to explain this aridity, a weakening of the AL may have contributed decreased moisture transport to the western United States.

Causes of Aleutian Low intensification from the mid-to late Holocene

Modern instrument observations show that the AL is sensitive to the dynamics of the upstream WJ over East Asia and the North Pacific Ocean (e.g., White and Barnett, 1972; Lau, 1988; Dole and Black, 1990; Nakamura et al., 2002; Yang et al., 2002; Athanasiadis et al., 2010; Park and An, 2014). Furthermore, a positive PNA mode is thought to follow intensified WJ conditions (Athanasiadis et al., 2010) due to enhanced wave activity along the WJ path over East Asia which becomes the trigger for PNA development (e.g., Mori and Watanabe, 2008). Hence, WJ behavior is linked closely to the state of the AL and its relationship with larger-scale atmospheric circulation modes.

Past WJ variations over East Asia have been reconstructed using Asian dust deposition flux, grain size, and provenance from terrestrial and lake sediments in China, Korea, and Japan (e.g., Ono et al., 1998; Sun, 2004; Lim and Matsumoto, 2006, 2008; Han et al., 2019), and marine sediments from the Japan Sea and northwestern Pacific Ocean (e.g., Janecek and

https://doi.org/10.1017/qua.2020.116 Published online by Cambridge University Press

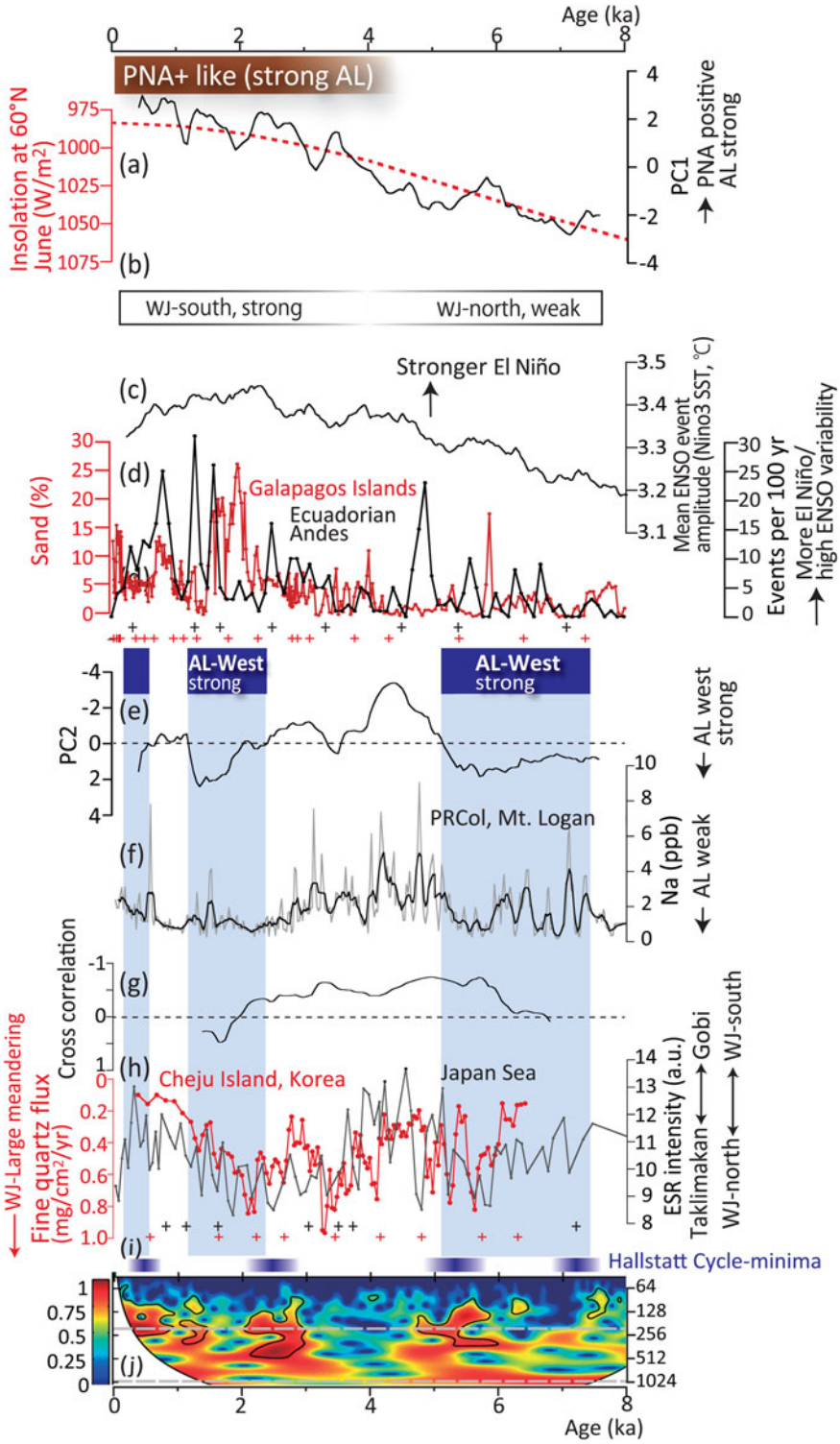

Figure 7. Time comparisons of proxy records of the Aleutian Low, the Westerly Jet, and El Niño–Southern Oscillation; (a) PC1 of $\delta^{18}O$ records (black line) and insolation at 60°N in June (red dotted line); (b) schematic orbital-scale trend of the WJ based on Rea and Leinen (1988), Nagashima et al. (2007), and Chen et al. (2019); (c) simulated Nino3 mean temperature amplitude of El Niño events in overlapping 500 year windows (Clement et al., 2000); (d) frequency of flood events at Laguna Pallcacocha in the Ecuadorian Andes (black line; Moy et al., 2002) and sand grain abundance at El Junco Crater Lake, Galapagos Islands (red line; Conroy et al., 2008); (e) PC2 of $\delta^{18}O$ records; (f) Na concentration from Mt. Logan ice core (gray line: raw data, black line: 5-pt moving average; Fisher et al., 2008); (g) cross-correlation between PC1 and 5-pt moving average of Mt. Logan Na using a 2000-yr moving window; (h) Electron spin resonance (ESR) signal intensity of quartz in core D-GC-6 from the Japan Sea (black line; Nagashima et al., 2013) and fine quartz flux deposited at Cheju Island, Korea (red line; Lim and Matsumoto, 2006, 2008); (i) solar minima of the Halstatt cycle (blue horizontal bars; Vasiliev and Dergechev, 2002); and (j) wavelet of total solar irradiance (Steinhilber et al., 2012). Age control points for selected records shown at the bottom of Figures 7d and 7h (cross marks).

https://doi.org/10.1017/qua.2020.116 Published online by Cambridge University Press

Rea, 1985; Rea and Leinen, 1988; Nagashima et al., 2007, 2011, 2013). Rea and Leinen (1988) reconstructed latitudinal changes of dust grain size using sediments from the northwestern Pacific Ocean (Fig. 1), and demonstrated a southerly shift of the northern margin of the WJ. Similar results were revealed by latitudinal changes of the grain size and deposition flux of Asian dust within Japan Sea sediments (Nagashima et al., 2007), where it was demonstrated that the WJ winter and spring paths shifts southward due to reduced summer insolation at 30°N, corresponding to the situation of the late Holocene. The history of WJ behavior has also been derived from aridity reconstructions of Central Asia, where the moisture is supplied by the WJ (inferred as westerlies in the original reference; e.g., Chen et al., 2019). According to Chen et al. (2019), a Holocene compilation of aridity records from Central Asia show wetter conditions during the late Holocene, which they interpret to reflect strengthened westerlies.

In summary, these reconstructions of the past WJ suggest a southward shift of the WJ path with probable intensification of wind speeds during the mid- to late Holocene, following the insolation decrease in summer and/or increase in winter (Fig. 7b). One of the proposed explanations for these orbital-scale WJ changes is that larger meridional temperature gradients exist due to stronger winter insolation during the late Holocene, which in turn generates a strengthened WJ over Central and East Asia (Chen et al., 2019). Reduced summer insolation during this same period probably attributes to the southern position of the WJ path, which would be analogues to the present seasonality of the WJ path that is characterized by a northward entrainment from winter to summer with the intensification of solar irradiation. These trends of WJ intensification along a southward path across the northwestern Pacific Ocean is characteristic of positive PNA conditions (Athanasiadis et al., 2010). These observations suggest that orbitally-driven WJ intensification and southward shift generate positive PNA-like (strong AL) state changes that are reflected in PC1 during the late Holocene (Figs. 7a–b).

Alternatively, the El Niño–Southern Oscillation (ENSO) is considered one of the most important factors driving North Pacific climate through its modulation of the PNA teleconnection pattern, which is sensitive to equatorial sea surface temperature (SST) anomalies (e.g., Horel and Wallace, 1981). The PNA tends to be positive (strong AL) during El Niño events due to higher SST in the tropical eastern Pacific (Renwick and Wallace, 1996). This can produce enhanced Rossby wave propagation from the tropical Pacific, directly exciting the PNA pattern (Horel and Wallace, 1981). Therefore, ENSO-like state changes have a high potential to generate AL variations between the middle and the late Holocene. This effect has been demonstrated by comparisons of $\delta^{18}O$ records from western North America and paleo-ENSO proxies (Barron and Anderson, 2011). To examine the possible effect of ENSO on our PCA composite of AL change, two ENSO proxy records (Moy et al., 2002; Conroy et al., 2008) and model simulations (Clement et al., 2000) were used for comparison. A sediment core from Laguna Pallcachocha in the Ecuadorian Andes contains a record of flood frequency preserved as hundreds of light-colored, inorganic clastic laminae, which generally correlate with known strong El Niño events in instrumental and historical records over the past 200 years (Moy et al., 2002). A complementary record of past ENSO variability has been interpreted from the grain size record of a sediment core derived from El Junco Crater Lake in the Galapagos Islands which shows several abrupt changes in lake level and precipitation during the Holocene (Conroy et al., 2008). Hydroclimatic model simulations suggest that the El Junco Lake level is sensitive to increases in precipitation associated with El Niño events, rising during wet El Niño events and falling during dry La Niña events (Conroy et al., 2008). The two records (Fig. 7d) show asynchronous centennial-scale peaks due to age uncertainty, but both show increases of ENSO variability with a greater abundance of El Niño-like conditions during the late Holocene. These trends are further supported by a numerical model of the tropical Pacific Ocean that includes orbital forcing that shows higher frequency and/or intensification of El Niño-like conditions as the Holocene progresses (Fig. 7c; Clement et al., 2000). According to Cane (2005), the weaker ENSO events during the early and middle Holocene were likely caused by stronger summer insolation, which helps to maintain a more northerly position of the Intertropical Convergence Zone. This is a barrier that prevents SST and wind conditions that favor the development of ENSO anomalies known as the Bjerknes feedback (Bjerknes, 1969). Inversely, the stronger ENSO events during the late Holocene were caused by weaker summer insolation or precessional-driven winter insolation increase in the tropic.

Based on this idea, ENSO intensification and frequent El Niño events during the late Holocene may also explain the PC1 change suggesting positive PNA-like state during the late Holocene. Consequently, either or both orbitally-driven changes in the WJ and ENSO generate preferential conditions for positive PNA modes and accompanied AL intensification during the mid- to late Holocene.

Causes of multi-centennial to millennial-scale Aleutian Low variability

Links with the Westerly Jet and ENSO

PC2 suggests AL intensifications and westward shifts during three time intervals: 7.5–5.1, 2.4–1.2, and 0.7–0.4 ka (Fig. 7e). These occurrences highlight the importance of identifying possible triggering mechanisms. The different spatial loading patterns observed between PC1 and PC2 (Figs. 4c–d) suggest that different mechanisms likely drive these two different modes of AL variability. The multi-centennial to millennial-scale AL variations in PC2 shows close synchronicity with WJ variations reconstructed from high-resolution Asian dust proxy records from the Japan Sea and Cheju Island, Korea (Lim and Matsumoto, 2006, 2008; Nagashima et al., 2013). An Asian dust provenance

https://doi.org/10.1017/qua.2020.116 Published online by Cambridge University Press

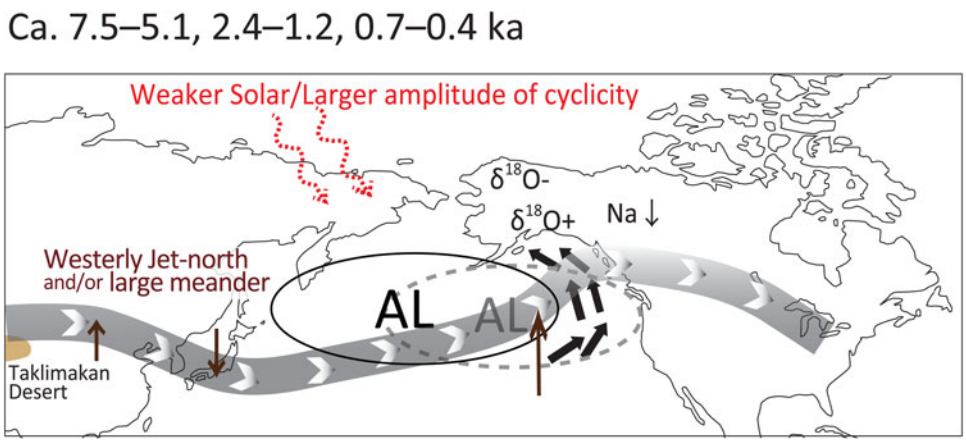

Figure 8. A schematic illustration of the Aleutian Low and the Westerly Jet behavior during Holocene intervals of PC2 maxima: 7.5–5.1, 2.4–1.2, and 0.7–0.4 ka. Corresponding changes in precipitation $\delta^{18}O$ and ice-core sodium concentration in North America are also depicted.

study that used sediment from the Japan Sea was used to reconstruct the WJ path over East Asia (Nagashima et al., 2011, 2013). Based on their interpretation, a predominance of dust from the Taklimakan Desert (Gobi Desert in southern Mongolia) represents the early (late) seasonal northward progression of the WJ path to the north of the Tibetan Plateau. This interpretation is based on the observation that dust emitted from the Gobi Desert is transported by near-surface northwesterly winds, while dust from the Taklimakan Desert is transported eastward by the WJ when it is shifted to the north of the Tibetan Plateau (Sun et al., 2001). Nagashima et al. (2013) identified a dominance of Asian dust from the Taklimakan Desert during ca. 7–5, 3.5–1.5, and after 0.4 ka (Fig. 7h) using Japan Sea sediment. These intervals overlap with those periods of multi-centennial to millennial-scale strengthened and westward shifts of the AL as interpreted above from PC2. The exception is the period around 0.5 ka, when Asian dust from the Gobi Desert dominates during a period with a strengthened and westward shifted AL, which is probably due to the age uncertainty of the Japan Sea sediment as there is no age constraint after 0.8 ka (Nagashima et al., 2013).

The flux and median diameter of fine fraction quartz deposited in a maar on Cheju Island since 6.5 ka have been used as indicators of WJ path changes (Lim and Matsumoto, 2006, 2008). The fine quartz fraction, which is composed of clay to fine-silt sized grains, is considered aeolian dust transported from the Taklimakan Desert by westerly winds (Lim and Matsumoto, 2006, 2008). The fine fraction quartz flux record deposited on Cheju Island exhibits similarities with the dust provenance study from the Japan Sea, as time intervals with higher dust flux correlates with periods of Taklimakan Desert-sourced dust over the Japan Sea (Fig. 7h; Lim and Matsumoto, 2008). These authors also showed that the grain size of this fine quartz fraction increases with higher flux rates, which suggests a longer duration and/or higher frequency of the WJ passing over both the Taklimakan Desert and Cheju Island. Both of these studies imply a predominant location for the WJ to the north of the Tibetan Plateau, with efficient dust transport to the Japan Sea and Cheju Island probably due to its larger meandering path (Lim and Matsumoto, 2008). This path is composed of a deeper northward ridge over the East Asia deserts and a deeper southward trough over the Japan Sea and Cheju Island, which frequently occur with a strengthened and westward shifted AL (Fig. 8).

The co-occurrence of northward shifts and/or large meanderings of the WJ with strengthened and westward shifted AL dynamics is similar to the typical atmospheric circulation pattern of the North Pacific sector that has been extracted statistically from the modern climate data (Athanasiadis et al., 2010). These authors used an EOF analysis of the zonal wind field at 250 hPa over the Pacific sector (120°E–105° W, 0°N–90°N) using the European Centre for Medium-Range Weather Forecast reanalysis during AD 1957–2002 to examine the relation between the WJ and North Pacific storm tracks. The negative polarity of EOF 2 is characterized by (i) a minor intensification of the WJ along its higher latitude margin over East Asia, and (ii) a large intensification over the eastern North Pacific Ocean along the northern branch of the WJ around 45°N (Athanasiadis et al., 2010), which is also known as an eddy-driven jet or a polar front jet. Abnormally strong storm tracks are embedded in the eddy-driven jet over the North Pacific (which is indicated by the negative polarity of EOF 2), which generate strengthened and northwestward-shifted AL. This pattern is distinct from the configuration associated with EOF 1, which is interpreted to show the WJ pattern associated with the PNA (Athanasiadis et al., 2010). The multi-centennial to millennial-scale WJ changes reconstructed from Asian dust provenance studies (Lim and Matsumoto, 2006, 2008; Nagashima et al., 2013) seem to be closely linked to the AL changes represented by PC2, which is distinctly different from the WJ-AL relationship reflected by PC1.

The influence of ENSO on the AL behavior reflected in PC2 is difficult to evaluate because the two ENSO proxy records show asynchronous peaks at multi-centennial to millennial scales (Fig. 7d; Moy et al., 2002; Conroy et al., 2008). However, the impact seems to be small or limited since

https://doi.org/10.1017/qua.2020.116 Published online by Cambridge University Press

neither of the ENSO proxy records show synchronicity with PC2 (Figs. 7d–e).

A role for solar forcing?

Meteorological records and reanalysis datasets have shown a sensitive response of WJ dynamics to the 11-year solar sunspot cycle (e.g., Arai, 1958; Labitzke, 1987; Kodera, 1995; Kodera and Kuroda, 2002). For longer timescales, spectral and wavelet analyses of paleoclimate proxy records representing WJ and AL behavior, such as flux of fine fraction quartz of lake sediment from Cheju Island (Lim and Matsumoto, 2008) and sodium concentration record of the Mt. Logan ice core (Osterberg et al., 2014), show cyclicity similar to the known solar activity cycles from multi-decadal to millennial timescales.

The dynamic mechanisms connecting solar activity and lower atmospheric circulation including WJ variability have been demonstrated by numerous studies (e.g., Haigh, 1996; Shindell et al., 2001, 2003; Kodera and Kuroda, 2002; Meehl et al., 2009; Gray et al., 2010; Ineson et al., 2011). One of these processes, the "top-down" mechanism, describes the response of stratospheric ozone to the ultraviolet (UV) radiation of the solar spectrum (Meehl et al., 2009; Gray et al., 2010). The small percentage of UV variation in the 11-year solar cycle generates changes in stratospheric circulation patterns (Frame and Gray, 2010; and references therein). These stratosphere changes then propagate downward into the tropospheric circulation, such as Hadley cell expansion/contraction (e.g., Gleisner and Thejll, 2003; Haigh 2003; Haigh et al., 2005) and WJ variability (Shindell et al., 2001, 2003). This linkage between solar activity and the WJ suggests that solar forcing is a plausible mechanism forcing the multi-centennial to millennial-scale atmospheric circulation changes related to the WJ and the AL.

Solar activity during the Holocene has been reconstructed by analyses of cosmic-ray produced radionuclides (^{14}C in tree rings and ^{10}Be in polar ice) using physics-based models (e.g., Solanki et al., 2004; Usoskin et al., 2016; Steinhilber et al., 2012). The periods of AL intensification and westward shifts inferred from the PC2 positive scores, taken together with the WJ northward shift and/or larger meandering path, appear to correlate with periods of solar minima associated with the Hallstatt cycle (2000–2400-year cyclicity, Fig. 7i; Vasiliev and Dergachev, 2002). Amplitudes of decadal to multi-centennial scale solar cycles have been shown to be modulated by the Hallstatt cycle, particularly with the largest amplitude events of the 210-year de Vries cycle (Figs. 7i–j; Eddy, 1997; Stuiver et al., 1991; Usoskin et al., 2016) occurring during Hallstatt cycle minima centered at approximately 7.2, 5.5, 2.5, and 0.5 ka (Fig. 7i; Vasiliev and Dergachev, 2002; Knudsen et al., 2009; Steinhilber et al., 2012; Usoskin et al., 2016; Usoskin, 2017). The periods of PC2 minima and related WJ anomalies overlap either or both the Hallstatt solar minima (Fig. 7i) and amplified de Vries cycle (Fig. 7j). This possible linkage between solar activity and the dynamic WJ-AL system is also supported by the 2000-year periodicity of PC2 ($p < 0.01$), extracted by a Lomb periodogram (Supplementary Figure 3). Hence it cannot be dismissed that external solar forcing can impact AL dynamics through changes of the WJ path over East Asia and the North Pacific Ocean. However, there is an inconsistency between the Hallstatt solar minima centered at 2.5 ka and a positive PC2 peak at the same time period, which highlights the need for additional new high-resolution and precisely dated WJ and AL paleoclimate records to further evaluate causal relationship between solar activity and linked WJ and AL variability.

CONCLUSIONS

Holocene variability of the AL and external forcing mechanism(s) were examined with a special focus on its relationship to the WJ. AL variability since 7.5 ka was reconstructed with multivariate PCA methods using seven previously published δ^{18}O records from sedimentary calcite, ice, and speleothems from Alaska, northwestern Canada, and the western United States. The extracted PC1 is characterized by a continuous increasing trend from the mid- to late Holocene, which appears to reflect intensified AL associated with a multi-millennial-scale shift in the PNA teleconnection pattern from a negative to positive-like state change. This interpretation is based on the comparison between the spatial distributions of individual δ^{18}O records, their respective PC1 loading scores, and the spatial patterns of both winter precipitation anomalies and simulated winter precipitation δ^{18}O anomalies associated with a positive PNA. This PNA-like change represented with PC1 seems likely related with either (or both): (i) orbitally-driven southward shift and intensification of the WJ; and/or (ii) ENSO intensification. This result also suggests that the modern AL system was established during the late Holocene.

The extracted PC2 shows dominance of multi-centennial to millennial-scale oscillations. The spatial loading pattern of PC2 and its comparison to winter precipitation amount and simulated winter precipitation δ^{18}O anomalies under different AL modes of variability suggests that PC2 reflects AL intensification with a westward shift during three periods since the mid-Holocene: 7.5–5.1, 2.4–1.2 and 0.7–0.4 ka. The timings of these AL anomalies are remarkably similar to periods when the WJ follows a more northerly route and/or large meander pathways over East Asia and the North Pacific Ocean. The paleoclimate records of these phenomena also show a similarity to the millennial-scale record of Hallstatt solar activity minima and the enhanced de Vries 210-year solar cyclicity. Together, these lines of evidence suggest changes in solar activity and/or the strength of cyclicity are associated with AL dynamics through interactions with the WJ path. The close linkage of the AL with the position of the WJ and its meandering pathways over East Asia and western North America suggest that the pacing of AL variability follows the rhythm of large-scale atmospheric circulation changes over the North Pacific Ocean and surrounding continents. These findings are critically important for understanding natural climate variability during the Holocene.

https://doi.org/10.1017/qua.2020.116 Published online by Cambridge University Press

ACKNOWLEDGMENTS

We thank Hitoshi Hasegawa, John Barron, and Jay Alder for providing useful input on early versions of this manuscript, as well as reviews by Daniel Mann, Thomas Cronin, and several anonymous reviewers. This research was supported by grants to Kana Nagashima (18H03370) from the Japan Society for the Promotion of Science. Support for Jason Addison was provided by the USGS Climate Research and Development Program. Any use of trade, firm, or product names is for descriptive purposes only and does not imply endorsement by the U.S. Government.

SUPPLEMENTARY MATERIAL

The supplementary material for this article can be found at https://doi.org/10.1017/qua.2020.116

REFERENCES

Addison, J.A., Finney, B.P., Jaeger, J.M., Stoner, J.S., Norris, R.D., Hangsterfer A., 2013. Integrating satellite observations and modern climate measurements with the recent sedimentary record: an example from Southeast Alaska. *Journal of Geophysical Research: Oceans* 118, 3444–3461.

Anderson, L., 2011. Holocene record of precipitation seasonality from lake calcite $\delta^{18}O$ in the central Rocky Mountains, United States. *Geology* 39, 211–214.

Anderson, L., 2012. Rocky Mountain hydroclimate: Holocene variability and the role of insolation, ENSO, and the North American Monsoon. *Global and Planetary Change* 92–93, 198–208.

Anderson, L., Abbott, M.B., Finney, B.P., Burns, S.J., 2005. Regional atmospheric circulation change in the North Pacific during the Holocene inferred from lacustrine carbonate oxygen isotopes, Yukon Territory, Canada. *Quaternary Research* 64, 21–35.

Anderson, L., Berkelhammer, M., Barron, J.A., Steinman, B.A., Finney, B.P., Abbott, M.B., 2016. Lake oxygen isotopes of Northern American Rocky Mountain hydroclimate: Holocene patterns and variability at multi-decadal to millennial time scales. *Global and Planetary Change* 137, 131–148.

Arai, Y., 1958. Characteristics of long waves in westerlies related to solar-activity. *Journal of Meteorological Society of Japan* 36, 46–54.

Athanasiadis, P.J., Wallace, J.M., Wettstein, J.J., 2010. Patterns of wintertime jet stream variability and their relation to the storm tracks. *Journal of the Atmospheric Sciences* 67, 1361–1381.

Bailey, H.L., Kaufman, D.S., Sloane, H.J., Hubbard, A.L., Henderson, A.C.G., Leng, M.J., Meyer, H., Welker, J.M., 2018. Holocene atmospheric circulation in the central North Pacific: a new terrestrial diatom and $\delta^{18}O$ dataset from the Aleutian Islands. *Quaternary Science Reviews* 194, 27–38.

Barron, J.A., Anderson, L., 2011. Enhanced late Holocene ENSO/PDO expression along the margins of the eastern North Pacific. *Quaternary International* 235, 3–12.

Beamish, R.J., Bouillon D.R., 1993. Pacific salmon production trends in relation to climate. *Canadian Journal of Fisheries and Aquatic Sciences* 50, 1002–1016.

Berkelhammer, M., Stott, L., Yoshimura, K., Johnson K., Sinha, A., 2012. Synoptic and mesoscale controls on the isotopic composition of precipitation in the western United States. *Climate Dynamics* 38, 433–454.

Biondi, F., Gershunov, A., Cayan, D.R., 2001. North Pacific decadal climate variability since 1661. *Journal of Climate* 14, 5–10.

Bjerknes, J., 1969. Atmospheric teleconnections from the equatorial Pacific. *Monthly Weather Review* 97, 163–172.

Bronk Ramsey, C., 2009. Bayesian analysis of radiocarbon dates. *Radiocarbon* 51, 337–360.

Cane, M.A., 2005. The evolution of El Niño, past and future. *Earth and Planetary Science Letters* 230, 227–240.

Cerny, B.A., Kaiser, H.F., 1977. A study of a measure of sampling adequacy for factor-analytic correlation matrices. *Multivariate Behavioral Research* 12, 43–47.

Chen, F., Chen, J., Huang, W., Chen, S., Huang, X., Jin, L., Jia, J. *et al.*, 2019. Westerlies Asian and monsoon Asia: spatiotemporal differences in climate change and possible mechanisms on decadal to sub-orbital timescales. *Earth-Science Reviews* 192, 337–354.

Clegg, B.F., Hu, F.S., 2010. An oxygen-isotope record of Holocene climate change in the south-central Brooks range, Alaska. *Quaternary Science Reviews* 29, 928–939.

Clement, A.C., Seager, R., Cane, M.A., 2000. Suppression of El Niño during the mid-Holocene by changes in the Earth's orbit. *Paleoceanography* 15, 731–737.

Compo, G.P., Whitaker, J.S., Sardeshmukh, P.D., Matsui, N., Allen, R.J., Allan, R.J., Yin, X. *et al.*, 2011. The twentieth century reanalysis project. *The Quarterly Journal of the Royal Meteorological Society* 137, 1–28.

Conroy, J.L., Overpeck, J.T., Cole, J.E., Shanahan, T.M., Steinitz-Kannan, M., 2008. Holocene changes in eastern tropical Pacific climate inferred from a Galápagos lake sediment record. *Quaternary Science Reviews* 27, 1166–1180.

Cook, E.R., Meko, D.M., Stahle, D.W., Cleaveland, M.K., 1999. Drought reconstructions for the continental United States. *Journal of Climate* 12, 1145–1162.

Cook, E.R., Woodhouse, C.A., Eakin, C.M., Meko, D.M., Stahle, D.W., 2004. Long-term aridity changes in the western United States. *Science* 306, 1015–1018.

D'Arrigo, R., Villalba, R., Wiles, G., 2001. Tree-ring estimates of Pacific decadal climate variability. *Climate Dynamics* 18, 219–224.

Di Lorenzo, E., Schneider, N., Cobb, K.M., Franks, P.J.S., Chhak, K., Miller, A.J., McWilliams, J.C. *et al.*, 2008. North Pacific Gyre Oscillation links ocean climate and ecosystem change. *Geophysical Research Letters* 35, L08607, doi:10.1029/2007GL032838.

Dole, R.M., Black, R.X., 1990. Life cycles of persistent anomalies. Part 2: The development of persistent negative height anomalies over the North Pacific Ocean. *Monthly Weather Review* 118, 824–846.

Eddy, J.A., 1997. The case of the missing sunspots. *Scientific American* 236, 80–88.

Ersek, V., Clark, P.U., Mix, A.C., Cheng, H., Edwards, L., 2012. Holocene winter climate variability in mid-latitude western North America. *Nature Communications* 3:1219, doi:10.1038/ncomms2222.

Ersek, V., Mix, A.C., Clark, P.U., 2010. Variations of $\delta^{18}O$ in rainwater from southwestern Oregon. *Journal of Geophysical Research* 115, D09109, doi:10.1029/2009JD013345.

Fisher, D., Osterberg, E., Dyke, A., Dahl-Jensen, D., Demuth, M., Zdanowicz, C., Bourgeois, J. *et al.*, 2008. The Mt Logan Holocene-late Wisconsinan isotope record: tropical Pacific-Yukon connections. *The Holocene* 18, 667–677.

Frame, T.H.A., Gray, L.J., 2010. The 11-year solar cycle in ERA-40 data: an update to 2008. *Journal of Climate* 23, 2213–2222.

Francis, R.C., Hare, S.R., 1994. Decadal scale regime shifts in the large marine ecosystems of the North-east Pacific: a case for historical science. *Fisheries Oceanography* 3, 279–291.

Gleisner, H., Thejll, P., 2003. Patterns of tropospheric response to solar variability. *Geophysical Research Letters* 30, doi:10.1029/2003GL017129.

Gray, L.J., Beer, J., Geller, M., Haigh, J.D., lockwood, M., Matthes, K., Cubasch, U., *et al*., 2010. Solar influences on climate. *Reviews of Geophysics* 48, RG4001, doi:10.1029/2009RG000282.

Haigh, J.D., 1996. The impact of solar variability on climate. *Science* 272, 981–984.

Haigh, J.D., 2003. The effects of solar variability on the Earth's climate. *Philosophical Transactions of the Royal Society* A 361, 95–111.

Haigh, J.D., Blackburn, M., Day, R., 2005. The response of tropospheric circulation to perturbations in lower-stratospheric temperature. *Journal of Climate* 18, 3672–3685.

Han, W., Lü, S., Appel, E., Berger, A., Madsen, D., Vandenberghe, J., Yu, L. *et al*., 2019. Dust storm outbreak in Central Asia after ~3.5 kyr BP. *Geophysical Research Letters* 46, 7624–7633.

Harada, N., Sato, M., Seki, O., Timmermann, A., Moossen, H., Bendle, J., Nakamura, Y. *et al*., 2012. Sea surface temperature changes in the Okhotsk Sea and adjacent North Pacific during the last glacial maximum and deglaciation. *Deep-Sea Research II* 61–64, 93–105.

Harbert, R.S., Nixon, K.C., 2018. Quantitative late Quaternary climate reconstruction from plant macrofossil communities in western North America. *Open Quaternary* 4, 1–13.

Horel, J.D., Wallace, J.M., 1981. Planetary-scale atmospheric phenomena associated with the Southern Oscillation. *Monthly Weather Review* 109, 813–829.

Ineson, S., Scaife, A.A., Knight, J.R., Manners, J.C., Dunstone, N.J., Gray, L.J., Haigh, J.D., 2011. Solar forcing of winter climate variability in the Northern Hemisphere. *Nature Geoscience* 4, 753–757.

Janecek, T.R., Rea, D.K., 1985. Quaternary fluctuations in the northern hemisphere trade winds and westerlies. *Quaternary Research* 24, 150–163.

Jones, M.C., Wooller, M., Peteet, D.M., 2014. A deglacial and Holocene record of climate variability in south-central Alaska from stable oxygen isotopes and plant macrofossils in peat. *Quaternary Science Reviews* 87, 1–11.

Kaiser, H.F. 1974. An index of factorial simplicity. *Psychometrika* 39, 31–36.

Kanamitsu, M., Kumar, A., Juang, H-M.H., Schemm, J-K., Wang, W., Yang, F., Hong, S-Y. *et al*., 2002. NCEP dynamical seasonal forecast system 2000. *Bulletin of the American Meteorological Society* 83, 1019–1038.

Kaplan, M.R., Wolfe, A.P., 2006. Spatial and temporal variability of Holocene temperature in the North Atlantic region. *Quaternary Research* 65, 223–231.

Kaufman, D.S., Axford, Y.L., Henderson, A.C.G., McKay, N.P., Oswald, W.W., Saenger, C., Anderson, R.S. *et al*., 2016. Holocene climate changes in eastern Beringia (NW North America) – A systematic review of multi-proxy evidence. *Quaternary Science Reviews* 147, 312–339.

Knudsen, M.F., Riisager, P., Jacobsen, B.H., Muscheler, R., Snowball, I., Seidenkrantz, M.S., 2009. Taking the pulse of the Sun during the Holocene by joint analysis of ^{14}C and ^{10}Be. *Quaternary Research Letters* 36, L16701, doi:10.1029/2009GL039439.

Kodera, K., 1995. On the origin and nature of the interannual variability of the winter stratospheric circulation in the northern hemisphere. *Journal of Geophysical Research* 100, 14,077–14,087.

Kodera, K., Kuroda, Y., 2002. Dynamical response to the solar cycle. *Journal of Geophysical Research* 107, 4749, doi:10.1029/2002JD002224.

Labitzke, K., 1987. Sunspots, the QBO, and the stratospheric temperature in the north polar region. *Geophysical Research Letters* 15, 535–537.

Latif, M., Barnett, T.P., 1994. Causes of decadal climate variability over the North Pacific and North America. *Science* 266, 634–637.

Lau, N-C., 1988. Variability of the observed midlatitude storm tracks in relation to low-frequency changes in the circulation pattern. *Journal of the Atmospheric Sciences* 45, 2718–2743.

Lim, J., Matsumoto, E., 2006. Bimodal grain-size distribution of aeolian quartz in a maar of Cheju Island, Korea, during the last 6500 years: its flux variation and controlling factor. *Geophysical Research Letters* 33, L21816, doi:10.1029/2006GL027432.

Lim, J., Matsumoto, E., 2008. Fine aeolian quartz records in Cheju Island, Korea, during the last 6500 years and pathway change of the westerlies over east Asia. *Journal of Geophysical Research* 113, D08106, doi:10.1029/2007JD008501.

Liu, Z., Tang, Y., Jian, Z., Poulsen, C.J., Welker, J.M., Bowen, G.J., 2017. Pacific North American circulation pattern links external forcing and North American hydroclimatic change over the past millennium. *Proceedings of the National Academy of Sciences of the United States of America* 114, 3340–3345.

Liu, Z., Yoshimura, K., Bowen, G.J., Buenning, N.H., Risi, C., Welker, J.M., Yuan, F., 2014. Paired oxygen isotope records reveal modern North American atmospheric dynamics during the Holocene. *Nature Communications* 5, 3701, doi:10.1038/ncomms4701.

MacDonald, G.M., Case, R.A., 2005. Variations in the Pacific Decadal Oscillation over the past millennium. *Geophysical Research Letters* 32, L08703, doi:10.1029/2005GL022478.

Mantua, N.J., Hare, S.R., Zhang, Y., Wallace, J.M., Francis, R.C., 1997. A Pacific interdecadal climate oscillation with impacts on salmon production. *Bulletin of the American Meteorological Society* 78, 1069–1080.

Mayewski, P.A., Rohling, E.E., Stager, J.C., Karlén, W., Maasch, K.A., Meeker, L.D., Meyerson, E.A. *et al*., 2004. Holocene climate variability. *Quaternary Research* 62, 243–255.

Meehl, G.A., Arblaster, J.M., Matthes, K., Sassi, F., van Loon, H., 2009. Amplifying the Pacific climate system response to a small 11-year solar cycle forcing. *Science* 325, 1114–1118.

Mori, M., Watanabe, M., 2008. The growth and triggering mechanisms of the PNA: a MJO-PNA coherence. *Journal of the Meteorological Society of Japan* 86, 213–236.

Moy, C.M., Seltzer, G.O., Rodbell, D.T., Anderson, D.M., 2002. Variability of El Niño/Southern Oscillation activity at millennial timescales during the Holocene. *Nature* 420, 162–165.

Nagashima, K., Tada, R., Matsui, H., Irino, T., Tani, A., Toyoda, S., 2007. Orbital- and millennial-scale variations in Asian dust transport path to the Japan Sea. *Palaeogeography, Palaeoclimatology, Palaeoecology* 247, 144–161.

Nagashima, K., Tada, R., Tani, A., Sun, Y., Isozaki, Y., Toyoda, S., Hasegawa, H., 2011. Millennial-scale oscillations of the westerly jet path during the last glacial period. *Journal of Asian Earth Sciences* 40, 1214–1220.

Nagashima, K., Tada, R., Toyoda, S., 2013. Westerly jet-East Asian summer monsoon connection during the Holocene. *Geochemistry Geophysics Geosystems* 14, 5041–5053.

Nakamura, H., Izumi, T., Sampe, T., 2002. Interannual and decadal modulations recently observed in the Pacific storm track activity and East Asian winter monsoon. *Journal of Climate* 15, 1855–1874.

Neukom, R., Steiger, N., Gomez-Navarro, J.J., Wang, J., and Werner, J.P., 2019. No evidence for globally coherent warm and cold periods over the preindustrial Common Era. *Nature* 571, 550–554.

Newman, M., Alexander M.A., Ault, T.R., Cobb, K.M., Deser, C., Di Lorenzo, E., Mantua, N.J. *et al*., 2016. The Pacific Decadal Oscillation, revisited. *Journal of Climate* 29, 4399–4427.

Ono, Y., Naruse, T., Ikeya, M., Kohno, H., Toyoda, S., 1998. Origin and derived courses of eolian dust quartz deposited during marine isotope stage 2 in East Asia, suggested by ESR signal intensity. *Global and Planetary Change* 18, 129–135.

Osterberg, E.C., Mayewski, P.A., Fisher, D.A., Kreutz, K.J., Maasch, KA., Sneed, S.B., Kelsey, E., 2014. Mount Logan ice core record of tropical and solar influences on Aleutian Low variability: 500–1988 A.D. *Journal of Geophysical Research: Atmospheres* 119, 11, 189–11, 204.

Osterberg, E.C., Winski, D.A., Kreutz, K.J., Wake, C.P., Ferris, D.G., Campbell, S., Introne, D., Handley, M., Birkel, S., 2017. The 1200 year composite ice core record of Aleutian Low intensification. *Geophysical Research Letters* 44, 7447–7454.

Overland, J.E., Adams, J.M., Bond, N.A., 1999. Decadal variability of the Aleutian Low and its relation to high-latitude circulation. *Journal of Clim*ate 12, 1542–1548.

Park, J.H., An, S.L., 2014. The impact of tropical western Pacific convection on the North Pacific atmospheric circulation during the boreal winter. *Climate Dynamics* 43, 2227–2238. doi:10.1007/s00382-013-2047-7.

Rea, D.K., Leinen, M., 1988. Asian aridity and the zonal westerlies: late Pleistocene and Holocene record of eolian deposition in the northwest Pacific Ocean. *Palaeogeography, Palaeoclimatology, Palaeoecology* 66, 1–8.

Renwick, J.A., Wallace, J.M., 1996. Relationships between North Pacific wintertime blocking, El Niño, and the PNA pattern. *Monthly Weather Review* 124, 2071–2076.

Rodinov, S.N., Overland, J.E., Bond, N.A., 2005. The Aleutian Low and winter climate conditions in the Bering Sea. Part I: Classification. *Journal of Climate* 18, 160–177.

Rodionov, S.N., Bond, N.A., Overland, J.E., 2007. The Aleutian Low, storm tracks, and winter climate variability in the Bering Sea. *Deep-Sea Research II* 54, 2560–2577.

Schiff, C.J., Kaufman, D.S., Wolfe, A.P., Dodd, J., Sharp, Z., 2009. Late Holocene storm-trajectory changes inferred from the oxygen isotope composition of lake diatoms, south Alaska. *Journal of Paleolimnology* 41, 189–209.

Shindell, D.T., Schmidt G.A., Mann, M.E., Rind, D., Waple A., 2001. Solar forcing of regional climate change during the Maunder Minimum. *Science* 294, 2149–2152.

Shindell, D.T., Schmidt G.A., Miller R.L., Mann, M.E., 2003. Volcanic and solar forcing of climate change during the preindustrial era. *Journal of Climate* 16, 4094–4107.

Shuman, B.N., Marsicek, J., 2016. The structure of Holocene climate change in mid-latitude North America. *Quaternary Science Reviews* 141, 38–51.

Solanki, S.K., Usoskin, I.G., Kromer, B., Schüssler, M., Beer, J., 2004. Unusual activity of the Sun during recent decades compared to the previous 11,000 years. *Nature* 431, 1084–1087.

Steinhilber, F., Abreu, J.A., Beer, J., Brunner, I, Christl, M., Fischer, H., Heikkilä, U. *et al*., 2012. 9,400 years of cosmic radiation and solar activity from ice cores and tree rings. *Proceedings of the National Academy of Sciences of the United States of America*, 109, 5967–5971.

Steinman, B.A., Abbott, M.B., 2013. Isotopic and hydrologic responses of small, closed lakes to climate variability: hydroclimate reconstructions from lake sediment oxygen isotope records and mass balance models, *Geochimica et Cosmochimica Acta* 105, 342–359.

Steinman, B.A., Pompeani, D.P., Abbott, M.B., Ortiz, J.D., Stansell, N.D., Finkenbinder, M.S., Mihindukulasooriya, L.N., Hillman, A.L., 2016. Oxygen isotope records of Holocene climate variability in the Pacific Northwest. *Quaternary Science Reviews* 142, 40–60.

Stuiver, M., Braziunas, T.F., Becker, B., Kromer, B., 1991. Climatic, solar, oceanic, and geomagnetic influences on late-glacial and Holocene atmospheric $^{14}C/^{12}C$ change. *Quaternary Research* 35, 1–24.

Sugimoto, S., Hanawa, K., 2009. Decadal and interdecadal variations of the Aleutian Low activity and their relation to upper oceanic variations over the North Pacific. *Journal of the Meteorological Society of Japan* 87, 601–614.

Sun, D., 2004. Monsoon and westerly circulation changes recorded in the late Cenozoic aeolian sequences of Northern China. *Global and Planetary Change* 41, 63–80.

Sun, J., Zhang, M., Liu, T., 2001. Spatial and temporal characteristics of dust storms in China and its surrounding regions, 1960–1999: relations to source area and climate. *Journal of Geophysical Research* 106, 10325–10333.

Ter Braak, C.F.J., and Prentice, I.C., 1988. A theory of gradient analysis. *Advances in Ecological Research* 18, 271–317.

Thompson, D.W.J., Wallace, J.M., 1998. The Arctic Oscillation signature in the wintertime geopotential height and temperature fields. *Geophysical Research Letters* 25, 1297–1300.

Trenberth, K.E., Hurrell, J.W., 1994. Decadal atmosphere-ocean variations in the Pacific. *Climate Dynamics* 9, 303–319.

Usoskin, I.G., 2017. A history of solar activity over millennia. *Living Reviews in Solar Physics* 14, A3.

Usoskin, I.G., Gallet, Y., Lopes, F., Kovaltsov, G.A., Hulot, G., 2016. Solar activity during the Holocene: the Hallstatt cycle and its consequence for grand minima and maxima. *Astronomy and Astrophysics* 587, A150.

Vachon, R.W., White, J.W.C., Gutmann, E., Welker, J.M., 2007. Amount-weighted annual isotopic ($\delta^{18}O$) values are affected by the seasonality of precipitation: a sensitivity study. *Geophysical Research Letters* 34, L21707, doi:10.1029/2007GL030547.

Vasiliev, S.S., Dergachev, V.A., 2002. The 2400-year cycle in atmospheric radiocarbon concentration: bispectrum of 14C data over the last 8000 years. *Annales Geophysicae* 20, 115–120.

Viau, A.E., Gajeski, K., Sawada, M.C., Bunbury, J., 2008. Low- and high-frequency climate variability in eastern Beringia during the past 25000 years. *Canadian Journal of Earth Sciences* 45, 1435–1453.

Wallace, J.M., and Gutzler, D.S., 1981. Teleconnections in the geopotential height field during the Northern Hemisphere winter. *Monthly Weather Review*s 109, 784–812.

White, W.B., Barnett, T.P., 1972. A servomechanism in the ocean/atmosphere system of the mid-latitude North Pacific. *Journal of Physical Oceanography* 2, 372–381.

Wooller, M.J., Kurek, J., Gaglioti, B.V., Cwynar, L.C., Bigelow, N., Reuther, J.D., Gelvin-Reymiller, C., Smol. J.P., 2012. An ~11,200 year paleolimnological perspective for emerging

https://doi.org/10.1017/qua.2020.116 Published online by Cambridge University Press

archaeological findings at Quartz Lake, Alaska. *Journal of Paleolimnology* 48, 83–99.

Yang, S., Lau, K.M., Kim, K.M., 2002. Variations of the East Asian Jet Stream and Asian-Pacific-American winter climate anomalies. *Journal of Climate* 15, 306–325.

Yoshimura, K., 2015. Stable water isotopes in climatology, meteorology, and hydrology: a review. *Journal of the Meteorological Society of Japan* 92, 513–533.

Yoshimura, K., Kanamitsu, M., Noone, D., Oki, T., 2008. Historical isotope simulation using reanalysis atmospheric data. *Journal of Geophysical Research* 113, D19108.

Yuan, F., Koran, M.R., Valdez, A., 2013. Late Glacial and Holocene record of climatic change in the southern Rocky Mountains from sediments in San Luis Lake, Colorado, USA. *Palaeogeography, Palaeoclimatology, Palaeoecology* 392, 146–160.

https://doi.org/10.1017/qua.2020.116 Published online by Cambridge University Press